Atmos. Chem. Phys. Discuss., 15, 34533–34604, 2015
www.atmos-chem-phys-discuss.net/15/34533/2015/
doi:10.5194/acpd-15-34533-2015

Atmospheric Chemistry and Physics Discussions

The contribution of soil biogenic NO emissions from a managed hyper-arid ecosystem to the regional NO_2 emissions during growing season

B. Mamtimin[1,2], M. Badawy[2,3], T. Behrendt[2,4], F. X. Meixner[2], and T. Wagner[1]

[1]Max Planck Institute for Chemistry, Satellite Research Group, Mainz, Germany
[2]Max Planck Institute for Chemistry, Biogeochemistry Department, Mainz, Germany
[3]Department of Geography, Faculty of Arts, Ain Shams University, Egypt
[4]Max Planck Institute for Biogeochemistry, Jena, Germany

Received: 16 November 2015 – Accepted: 24 November 2015
– Published: 10 December 2015

Correspondence to: B. Mamtimin (buhalqem.mamtimin@mpic.de)

Published by Copernicus Publications on behalf of the European Geosciences Union.

Abstract

A study was carried out to understand the contributions of soil biogenic NO emissions from managed (fertilized and irrigated) hyper-arid ecosystem in NW-China to the regional NO_2 emissions during growing season. Soil biogenic NO emissions were quantified by laboratory incubation of corresponding soil samples. We have developed the Geoscience General Tool Package (GGTP) to obtain soil temperature, soil moisture and biogenic soil NO emission at oasis scale. Bottom-up anthropogenic NO_2 emissions have been scaled down from annual to monthly values to compare mean monthly soil biogenic NO_2 emissions. The top-down emission estimates have been derived from satellite observations compared then with the bottom-up emission estimates (anthropogenic and biogenic). The results show that the soil biogenic emissions of NO_2 during the growing period are (at least) equal until twofold of the related anthropogenic sources. We found that the grape soils are the main summertime contributor to the biogenic NO emissions of study area, followed by cotton soils. The top-down and bottom-up emission estimates were shown to be useful methods to estimate the monthly/seasonal cycle of the total regional NO_2 emissions. The resulting total NO_2 emissions show a strong peak in winter and a secondary peak in summer, providing confidence in the method. These findings provide strong evidence that biogenic emissions from soils of managed drylands (irrigated and fertilized) in the growing period can be much more important contributors to the regional NO_2 budget (hence to regional photochemistry) of dryland regions than thought before.

1 Introduction

Atmospheric carbon monoxide, methane, and volatile organic compounds are oxidized by the hydroxyl and other radicals through various catalytic cycles (Crutzen, 1987). In these cycles, nitrogen oxides (NO_x) are key catalysts, and their ambient concentrations determine whether ozone (O_3) is generated or destroyed in the troposphere (Chamei-

ACPD
15, 34533–34604, 2015

des et al., 1992). The present evolution of anthropogenic as well as biogenic NO_x sources triggers a potential increase of global tropospheric O_3 concentrations. NO_x in the troposphere originate mostly as NO, which photo-stationary equilibrates with NO_2 within a few minutes. According to recent estimates (Kasibhatla et al., 1993; Davidson and Kingerlee, 1997; Denman et al., 2007; Feig et al., 2008), anthropogenic sources amount to 45–67 % of the mid 2000s total global NO_x emissions (42–47 $Tg\,a^{-1}$, in terms of mass of N). Other globally important sources are soil biogenic NO emission (10–40 %), biomass burning (13–29 %) and lightning (5–16 %). The considerable uncertainty about the range of soil biogenic NO emissions stems from widely differing estimates of the NO emission. Based on field measurements world-wide Davidson and Kingerlee (1997) estimated the global NO soil source strength to be 21 $Tg\,a^{-1}$ (with an error margin of 4 to 10 $Tg\,a^{-1}$, 40 % of the total), while the 4th IPCC estimate is 8.9 $Tg\ a^{-1}$ (Denman et al., 2007) up from the 3th IPCC estimate of 5.6 $Tg\ a^{-1}$ (IPCC, 2001). Moreover, the uncertainties in the NO emission data from semi-arid, arid, and hyper-arid regions are very large (mainly due to a very small number of measurements being available). In this context, one should be aware, that approximately 40 % of planet Earth's total land surface consists of semi-arid, arid and hyper-arid land and more than 30 % of the world's inhabitants live in hyper-arid, arid and semiarid regions (Lai, 2001).

In many parts of the world's drylands land-cover is strongly changing due to the encroachment of desert by bushy vegetation (desert → dryland farming; bushy → dryland farming). This leads and will lead to dramatic changes in soil microbial production and consumption of NO. Consequently, it will have a strong impact on the (at least) regional budgets of those reactive trace gases (NO_x, O_3, volatile organic compounds (VOC), etc.) which involved in the tropospheric oxidizing capacity. For this reason, it is necessary to quantify the NO emissions from both, natural and agricultural managed soils of the drylands.

Recently, Oswald et al. (2013) convincingly pointed out, that (a) the release of odd reactive nitrogen gases from soils due to microbial action is not confined to NO only, and (b) about equal amounts of gaseous nitrous acid (HONO) are simultaneously emit-

ACPD
15, 34533–34604, 2015

ted along with NO. In addition, NO production from the HONO photolysis in day time is attributed to the total production of NO_x emission. Therefore, it is meaningful to include HONO emissions to any estimates of biogenic total reactive nitrogen emissions from soil.

The biogenic emission of NO (as well as HONO) depends crucially on soil temperature and soil moisture, because these factors affect the availability of organic compounds and the microbial activity in the soil (Conrad, 1996; Meixner and Yang, 2006; Ludwig et al., 2001; Oswald et al., 2013). Sufficient soil moisture, high soil temperatures, and regular supply of nutrients (N containing fertilizer) are optimum conditions for soil biogenic NO (and HONO) emissions, particularly from arid and hyper-arid land.

An oasis is an agriculturally used area in a desert region. The intensification (economically driven) of oasis agriculture, however, needs enlargement of the arable land area, enhancement of necessary irrigation, and increase of fertilizer use, which leads inevitably to increasing soil biogenic NO (and HONO) emissions. Microbial processes, which underlay NO production (and NO consumption) in soils (e.g., nitrification, denitrification) are confined to the uppermost soil layers (< 0.05 m depth, Rudolph et al., 1996). The most direct method for the characterization of these processes and the quantification of the NO (and HONO) release from soils is usually realized by laboratory incubation of soil samples taken from top soil layers. In those laboratory incubation systems, the net release rate of NO is determined from the NO concentration difference between incoming and outgoing air. The application of this method in the past has proved that the release of NO can be described by specific and unique functions of soil moisture, soil temperature, and ambient NO concentration (Otto et al., 1996; van Dijk et al., 2002; Meixner and Yang, 2006; Feig et al., 2008; Behrendt et al., 2014; Mamtimin et al., 2015).

Due to the industrialization of Chinese drylands and also to the intensification of their agriculture, not only large anthropogenic NO_x emissions from growing oasis cities are expected, but also current land use will also intensify the "hot spot" character of soil biogenic NO emissions from oases. The general aim of the present study is to determine

ACPD
15, 34533–34604, 2015

the contributions of soil biogenic NO emission of a selected oasis in the Taklimakan desert to the regional NO_2 emissions during the growing season. For that, we concentrate (a) on biogenic NO fluxes derived from laboratory incubation measurements of soil samples, (b) on up-scaling the laboratory results to the spatial level of an oasis by a Geoscience General Tool Package (GGTP; specifically developed for all GIS up-scaling procedures of this study), (c) on the estimation of anthropogenic NO_2 emissions of the oasis based on energy consumption and NO_2 emission factors of different sectors and fuel types, (d) on the quantitative comparison of the derived results to satellite observations (OMI) of the vertical NO_2 column densities at regional scale, (e) on the estimation of top-down (satellite derived) and bottom-up (biogenic and anthropogenic) NO_2 emissions.

2 Materials and methods

2.1 Site description and soil sampling

The study area "Tohsun oasis" (Fig. 1) is a hyper-arid region located in the Xinjiang Uyghur Autonomous Region of P.R. China (Mamtimin et al., 2005). The Tohsun oasis belongs administratively to Turpan County with Turpan City as capital (50 km NE from Tohsun oasis). The Tohsun oasis has an extension of 1479 km^2, a population of 138 thousand, and topographically constitutes the deepest point of P.R. China (154 m below sea-level; Pu, 2011). Major landform types of the Tohsun oasis are sandy-desert and Gobi-desert (stone desert), surrounded on three sides by the mountains of Bogda (north), Qoeltagh (south), and Alagou (west). Topographically, the Tohsun oasis slopes down from northwest to southeast. According to the Koeppen classification (Kottek et al., 2006), the climate of the Tohsun oasis is classified as "cold desert"; i.e. hot summers (July: 33 °C), cold winters (January: −6 °C), and very low precipitation. Mean annual potential evaporation is about 3400 mm (s. Fig. 2), while the mean annual precipitation is as low as 7 mm.

ACPD
15, 34533–34604, 2015

The mean monthly precipitation for Tohsun (not shown in Fig. 2) is extremely low: rainfall in June and July is about 2 mm, in January, August, and 1 September mm, respectively; and there is no rain for the rest of the year. Agriculture played and plays a significant role in Tohsun oasis; it was one of the most flourishing oases on the ancient Silk Road (Weggel, 1985). Due to the substantial lack of rainfall, regular dry-land farming is impossible without massive irrigation. Water supplies for irrigated agriculture are dependent on groundwater (pumping-wells), and on the Bai Yanggou River which originates from the Bogda Mountain. The Bai Yanggou River is temporary, defined by the strong seasonal pattern of snow-melt and rain in the mountains (Mamtimin, 2005).

Tohsun oasis' agriculture is dominated by intensive mono-cultivation of grapes and cotton. Grapes from the Turpan country are naturally dried to raisins which are sold on the Chinese internal market and also exported to some Asian countries (Jin, 2011; Pu, 2011). Grapes from Turpan County account for 52 % of grape production in the Xinjiang Uyghur Autonomous Region, and for 20 % of entire China. There, more than 100 small and medium size companies are engaged in raisin processing (Wan, 2012). In 2008, Turpan's raisin production was 130 000 t which accounted for more than 90 % of all raisins produced in P.R. China (Wan, 2012; Li et al., 2012; Jin, 2011; Pu, 2011). Approximately 40 % of Turpan's grape production is from the Tohsun oasis (Pu, 2011). To raise the yields of grapes and cotton, the corresponding cultivation techniques have been optimized, which resulted in the application of nitrogen containing fertilizers.

Soil samples from the study area were collected in 2010 from a total of three sites of Tohsun's cotton fields, and from a total of two sites of corresponding grape fields (for sample locations, see Fig. 1). In this study, we also used soil samples from the non-fertilized desert ecosystem as reference, where the desert soil data was adapted from the study Mamtimin et al. (2015).

2.2 Remote sensing and accompanying data

Remote sensing data from both Landsat and Aura satellites (measurements by the Ozone Monitoring Instrument, OMI) were used in combination with a Geographical In-

ACPD
15, 34533–34604, 2015

formation System (GIS). Landsat images, provided by United States Geological Survey, are widely applicable for purposes like our study because of their rather high spatial resolution (30–15 m). Since the aim of our study is the quantification of biogenic NO emissions from intensively managed arid soils, the consideration of the growth state of the corresponding agro-ecosystems is important. For the representation of the different seasons we selected four individual months: April (spring) for the begin, July, August (summer) for the middle, and September (autumn) for the end of the vegetation period. The winter season was not considered, as most of the agro-ecosystems are frozen, hence any microbial activities are negligible. As proposed by many authors (Schott et al., 1985; Markham et al., 1986; Irish, 2003; Chander et al., 2003; Zeng et al., 2004) we derived for each season areal distributions of land surface temperature (LST), soil moisture index (SMI), and land cover types from corresponding satellite data using remote sensing digital image processing. For the selection of Landsat images we confined ourselves to the year 2010 when we have taken the soil samples.

Tropospheric NO_2 column densities derived from the OMI satellite instrument (DOMINO version 2.0, Boersma et al., 2011) were used for comparison with the bottom-up emission estimates (biogenic and anthropogenic). OMI is operated in a sun-synchronous orbit such that measurements are taken at about 13:45 LT. The seasonal patterns of satellite derived NO_2 column densities were evaluated using cloud-free measurements from 2006 to 2010. Four different areas were selected to represent (1) typical agricultural areas (study area), (2) mixed land use areas (agricultural and small urban), (3) large urban areas, and (4) desert. The seasonal patterns of satellite derived NO_2 column densities were evaluated using measurements from 2006 to 2010.

For the estimation of anthropogenic sources of NO_x, we used fossil fuel consumption data from different economic sectors (manufacturing, electricity, transportation and domestic) which were obtained from the Xinjiang Statistical Yearbooks (Jin et al., 2009, 2011) and the Turpan Statistical Yearbooks (Pu, 2009, 2011). The emission-reduction coefficient for coal-fired thermal power industry was taken from "China Electric Power Yearbook" (Zhou, 2006). The land use map of Xinjiang (1 : 10 000 000, 2010) and the

ACPD
15, 34533–34604, 2015

Traffic Map of Tohsun (1 : 1 050 000, 2010) were involved within this study as additional tools for land use classification.

The meteorological data set (1971–2005) of the Tohsun County Meteorological Station (42.7833° N, 88.6500° E; +1 m a.s.l.) was supplied by the Xinjiang Meteorological Bureau. It contains monthly mean (1971–2005) data of air temperature, precipitation, evaporation, wind speed and direction. Unfortunately, soil moisture content and soil temperature have not been measured routinely at Tohsun County Meteorological Station.

Satellite derived LST and SMI data, from six individual Landsat images of the Tohsun oasis (25 April, 28 July, 13 and 21 August, 6 and 22 September 2010) were used for the validation of the satellite data by in situ data of soil temperature and soil moisture content. Corresponding continuous in situ measurements have been performed with a suitable sensor (MSR® 165 data logger; Rotronic, Switzerland) which has been buried at the site of Tohsun County Meteorological Station at 2.5 cm depth between July and September 2010. While soil temperature data was measured directly, data of gravimetric soil water content was calibrated vs. relative humidity of the soil air by a vapor analyzer (VSA, Decagon, USA).

The estimation of the seasonal variation of biogenic NO emissions requires temporally high-resolution data of (a) soil temperature, (b) gravimetric soil water content, and (c) amplification of NO fluxes due to the application of fertilizer (s. Sect. 2.5.2). While soil temperature data could be provided by measurements, data of gravimetric soil moisture content for “cotton” and “grapes” fields had to be assimilated from (a) information of irrigation cycles obtained by personal communication (2010) with farmers in the Tohsun oasis, and (b) from in situ measurements of relative humidity of soil air which were adapted from observations at the oases of Kuche and Minfeng (see Sect. 2.4.5). Suitable, fertilizer amount dependent “amplification factors” have been deduced from recent investigations on the impact of N-containing fertilizers on NO fluxes from arable soils of the Taklimakan region by Fechner (2014).

ACPD
15, 34533–34604, 2015

2.3 Laboratory determination of the net NO release and net potential NO fluxes

During the last two decades, this laboratory method has been used to measure the net NO release from soil (Yang and Meixner, 1997; Otter et al., 1999; Kirkman et al., 2001; Feig et al., 2008; Yu et al., 2008; Ashuri, 2009; Gelfand et al., 2009; Bargsten et al., 2010; Behrendt et al., 2014; Mamtimin et al., 2015). However, today's knowledge of soil biogenic NO emission rates from managed arid soils are very limited (c.f. Behrendt et al., 2014; Mamtimin et al., 2015; Delon et al., 2015).

The net release of NO from soil is the result of microbial production and consumption processes which occur simultaneously (Conrad, 1996). In our study, we investigated net NO releases (J_{NO} in terms of mass of nitric oxide per mass of dry soil and time), as well as potential NO fluxes (F_{NO}; in terms of mass of nitric oxide per area and time) of cotton, grapes and desert soils. The methodology for the laboratory soil measurements which is used in the frame of this study, is described in great detail in Behrendt et al. (2014) and Mamtimin et al. (2015). By application of the laboratory dynamic chamber method, the net potential NO flux F_{NO} (ng m^{-2} s^{-1}, in terms of mass of NO) is defined by

$$F_{NO}\left(\theta_g, T_{soil}\right) = J_{NO}\left(\theta_g, T_{soil}\right) \frac{m_{soil}}{A} \quad (1)$$

where J_{NO} (in ng kg^{-1} s^{-1}) is derived from the laboratory measurements, as well as the dimensionless gravimetric soil moisture θ_g. The soil temperature T_{soil} (in °C), the total mass of the dry soil sample m_{soil} (in kg), and the cross section of the dynamic chamber A (in m^2) were directly measured.

Soil moisture and soil temperature had been identified as the most dominant influencing factors of the net NO release; therefore, J_{NO} is usually parameterized by these two quantities (Yang and Meixner, 1997; Otter et al., 1999; Kirkman et al., 2001; van Dijk et al., 2002; Meixner and Yang, 2006; Yu et al., 2008, 2010; Feig et al., 2008; Ashuri, 2009; Gelfand et al., 2009; Bargsten et al., 2010). While the dependence of

ACPD
15, 34533–34604, 2015

J_{NO} on T_{soil} is exponential, J_{NO} has θ_g the form of an optimum curve. These dependencies are described by two explicit dimensionless functions, the so-called optimum soil moisture curve $g(\theta_g)$ and the exponential soil temperature curve $h(T_{soil})$ which are described in detail by Behrendt et al. (2014). Introducing $\theta_{g,0}$, the so-called optimum gravimetric soil moisture content (i.e., where the maximum NO release has been observed), and $T_{soil,0} = 25\,^{\circ}C$ as the reference soil temperature, the net potential NO flux, specific for the soils of each land use type i (i: grape fields, cotton fields, desert) is given by

$$F_{NO,i}\left(\theta_{g,i}, T_{soil,i}\right) = J_{NO,i}\left(\theta_{g,0,i}, T_{soil,0,i}\right)\, g_i\left(\theta_{g,i}\right)\, h_i\left(T_{soil,i}\right) \quad (2)$$

2.4 Development of the Geoscience General Tool Package (GGTP)

The Landsat TM/ETM+ sensors acquire land surface information and store it as a digital number (DN) which ranges between 0 and 255; Landsat images are widely applied for the estimation of biospheric applications, such as the Normalized Differenced Vegetation Index (NDVI), Land Surface Temperature (LST), Soil Moisture Index (SMI), and fluxes of matter between different ecosystems, etc. (Goward and Williams, 1997; Liang et al., 2002; Lu et al., 2002). In order to upscale biogenic NO emissions derived from laboratory measurements to the oasis level, we have developed a tool, the so-called "Geoscience General Tool Package (GGTP)" for ARCGIS 10.x using model builder and python 2.7. By knowing LST, SMI and the land use type specific parameterized soil biogenic NO fluxes for each field, the net NO fluxes of each pixel of the oasis were calculated in a fine scale matrix (30 m × 30 m) within the GGTP framework. For that, GGTP has been specifically developed, namely to process digital images (e.g. Landsat images) and to model 2-D distributions of biogenic NO emission. In particular, the following calculation (sub-) schemes have been implemented.

ACPD
15, 34533–34604, 2015

2.4.1 Landsat-7 SLC-off gap filling

The Landsat 7 Enhanced Thematic Mapper Plus (ETM+) scan line corrector (SLC) failed on 31 May 2003, causing that scanning patterns exhibited wedge-shaped, scan-to-scan gaps. The ETM+ has continued to acquire data with the SLC powered off, leading to images that are missing approximately 22 % of the usual scene area. Therefore, the US Geological Survey (USGS) provided an additional bit mask (gap files) that identifies the location of the image gaps. We used a local linear histogram matching radiometric algorithm to create a gap-filled output product (Storey et al., 2005; Storey, 2011). This technique was proposed by USGS/NASA and consists of a localized linear transformation performed in a moving window. The implementation of this algorithm requires both image products, SCL-off and SCL-on scenes. For that, we used the Landsat ETM+ SCL-on scene of August 2000. The gap filling was implemented by calculation of (a) the gain and bias, based on the mean and standard deviation of common pixels, and (b) the missing pixel value, using the derived gain and bias as shown by Storey et al. (2005, 2011) and Chen et al. (2011).

2.4.2 Calculation of NDVI Surfaces ($NDVI_{surf}$)

The NDVI differentiates between green vegetation and soil background, which is useful for the retrievals of land surface emissivity and soil moisture (Van de Griend et al., 1993; Jackson et al., 2004; Wang et al., 2007; Yilmaz et al., 2008). Erroneous NDVI estimates can directly affect biophysical parameters such as temperature and moisture which are extracted directly and indirectly from these values: pre-processing of atmospheric corrections of remotely sensed data is essential (Jensen, 2005). One of these atmospheric corrections is the absolute radiometric correction which aims to turn the raw digital numbers (DN), recorded by a remote sensing instrument into scaled surface reflectance values (Du et al., 2002; Jensen, 2005). The NDVI can be calculated from Landsat image bands ETM 3 and ETM 4 (near-infrared and red); in this study atmospheric corrections for bands ETM3 and ETM4 were performed (described in Sect. “Top

ACPD
15, 34533–34604, 2015

of atmosphere (TOA) reflectance (ρ_{TOA})"). The calculated NDVI values, which are then representing natural surfaces, are called $NDVI_{surf}$ (Sobrino et al., 2004).

At-sensor spectral radiance (L_λ)

The at-sensor spectral radiance (L_λ) is used to characterize the amount of light at the sensor and it is a scientific term used to describe the power of radiation. The calculation of L_λ is a primary step in converting image data from multiple sensors into a common physical scale which can be implemented by radiometric calibration. During this calibration process, raw DN transmitted from the satellite instrument converted to calibrated DN (Q_{cal}). DN of Landsat images represent the dimensionless integer that a satellite uses to record relative amounts of radiance. For radiometric calibration, the following steps were involved: (a) pixel values of DN are converted into absolute spectral radiance by using a 32-bit floating point calculation, (b) absolute radiances are then scaled to 8-bit values representing calibrated DN Q_{cal}, and (c) the conversion from Q_{cal} products back to at-sensor spectral radiance (L_λ). For conversion of Q_{cal} to L_λ, the following equation is used (Chander and Markham, 2003):

$$L_\lambda = (L_{max\lambda} - L_{min\lambda}/Q_{calmax}) \times Q_{cal} + L_{min\lambda} \quad (3)$$

where L_λ is the spectral radiance at the sensor (power per steradian, μm and m^2, i.e. W m^{-2} sr^{-1} μm^{-1}), Q_{cal} is the calibrated pixel value (dimensionless), and Q_{calmax} is the maximum calibrated pixel value (corresponding to $L_{max\lambda}$), $L_{max\lambda}$ and $L_{min\lambda}$ (W m^{-2} sr^{-1} μm^{-1}) are the spectral radiances scaled to Q_{calmax} and Q_{calmin}, respectively. The lower and upper limit rescaling factors ($L_{max\lambda}$ and $L_{min\lambda}$) were obtained from the supplemented header file of the satellite images.

Top of atmosphere (TOA) reflectance (ρ_{TOA})

To obtain NDVI values, the calculated radiances need to be converted into an at-sensor reflectance (spectral reflectance value), also called top of atmosphere reflectance

ACPD
15, 34533–34604, 2015

(ρ_{TOA}). The top of atmosphere (TOA) correction converts the at-sensor spectral radiance (L_λ) to the top of atmosphere reflectance (ρ_{TOA}), and this process is one of the atmospheric correction methods used to reduce scene-to-scene variability (Markham and Barker, 1986; Chander and Markham, 2003; Chander et al., 2009). This is important when comparing scenes to scenes or producing image mosaics. The dimensionless TOA reflectance, called ρ_{TOA}, is defined as follows:

$$\rho_{TOA} = \frac{\pi \cdot L_\lambda \cdot d^2}{E_{SUN,\lambda} \cdot \cos(\theta_s)} \quad (4)$$

where L_λ is the spectral radiance at the sensor (s. Eq. 3), d is the Earth–Sun distance (astronomical units) depending on the day of the year (DOY), $E_{SUN,\lambda}$ is the mean exoatmospheric solar irradiance ($W\,m^{-2}\,\mu m^{-1}$), and $\cos(\theta_s)$ is the cosine of the sun zenith angle, which is equal to sine of the solar elevation angle. The solar elevation angle at each Landsat scene center is typically stored in the Level 1 product header file of each Landsat Image (obtained from USGS Earth Explorer or GloVis online interfaces under the respective scene metadata).

At-surface reflectance (ρ_{surf})

Basically, it is possible to derive the NDVI from the at sensor corrected reflectance (ρ_{TOA}), which is then called $NDVI_{TOA}$ (Sobrino et al., 2004). However, the NDVI is based on surface reflectance, thus, it is more accurate to convert the at sensor reflectance (TOA) into the at-surface reflectance. Then, the estimated NDVI values would represent the natural surface, and are called $NDVI_{surf}$. As described by Sobrino et al. (2004), the at-surface reflectance is:

$$\rho_{surf}^{ETM3} = 1.0705 \times \rho_{TOA}^{ETM3} - 0.0121 \quad (5a)$$

$$\rho_{surf}^{ETM4} = 1.0805 \times \rho_{TOA}^{ETM4} - 0.0047 \quad (5b)$$

ACPD
15, 34533–34604, 2015

where ρ_{surf}^{ETM3} and ρ_{surf}^{ETM4} are the at-surface reflectivities, and ρ_{TOA}^{ETM3}, ρ_{TOA}^{ETM4} are the corresponding TOA reflectivities for the ETM band 3 and ETM band 4, respectively, calculated by Eq. (4).

$NDVI_{surf}$ is then calculated as follows:

$$NDVI_{surf} = \left(\rho_{surf}^{ETM4} - \rho_{surf}^{ETM3}\right) / \left(\rho_{surf}^{ETM4} + \rho_{surf}^{ETM3}\right) \quad (6)$$

Theoretically, $NDVI_{surf}$ values, which constitute a ratio, range from −1 to 1; water typically has an NDVI value less than 0, bare soils range between 0 and 0.1 and vegetation is represented by NDVI > 0.1.

2.4.3 Land surface emissivity and land surface temperature T_s

Knowledge of the land surface emissivity is highly indispensable to retrieve the land surface temperature (T_s) and soil moisture index (SMI) from remotely sensed data. Land surface emissivity (ε) is known as the relative fraction of a surface emission compared to the emission of a black body of the same temperature. As the land cover varies greatly from place to place, land surface emissivity (LSE) widely varies from one location to another. Van de Griend and Owe (1993) found a high correlation between measured emissivity and NDVI obtained from red and near-infrared (NIR) spectral reflectance, expressed by the following relation:

$$\varepsilon = 1.0094 + 0.047 \ln NDVI_{surf} \quad (7)$$

Note, that this relationship is not valid for areas characterized by highly dense vegetation cover. Since the NDVI values in our study area range between 0 and 0.7, application of Eq. (7) is certainly justified in the case of the Tohsun oasis. For the calculation of LST we made use of Stefan–Boltzmann's law:

$$B = \varepsilon \sigma T_s^4 = \sigma T_B^4 \quad (8)$$

ACPD
15, 34533–34604, 2015

where, B is the total amount of the emitted radiation (W m^{-2}), ε is the land surface emissivity (obtained from Eq. 7), σ is the Stefan–Boltzmann constant (5.67×10^{-8} W m^{-2} K^{-4}), and T_s and T_B are the land surface temperature and the at-sensor brightness temperature (K). Therefore the land surface temperature T_s is defined as:

$$T_s = \frac{1}{\varepsilon^{0.25}} T_B \quad (9)$$

The at-sensor brightness temperature can be calculated from the satellite image's thermal band of high gain mode (band 6.2). In the case of Landsat satellite series, Schott and Volchok (1985), Markham and Barker (1986), Wucelic et al. (1989), Irish (2003) and Chander et al. (2009) proposed a simplified formula for the estimation of the at-sensor brightness temperature as follows:

$$T_B = \frac{K2}{\ln\left(\frac{K1}{L_\lambda} + 1\right)} \quad (10)$$

Here K1 (W m^{-2} sr^{-1} μm^{-1}) and K2 (K) are calibration constants, and L_λ the spectral radiance at the sensor's aperture. For Landsat-7 ETM+ images, K1 and K2 have numerical values of 666.09 and 1282.71, respectively.

Generally, T_s is defined as the so-called "skin temperature" of the surface. For the bare soil surface, it is the soil temperature; for the vegetated areas, T_s can be considered as the average temperature of the vegetation body and the soil surface below the vegetation.

2.4.4 Soil Moisture Index (SMI)

In several studies (Goward et al., 2002; Lambine and Ehrlich, 1996; Sandholt et al., 2002; Wang et al., 2007), the correlation between T_s and NDVI has been shown to be related to surface soil moisture. Several approaches were tested to develop and improve soil moisture estimates from the space of T_s and NDVI (Carlson et al., 1995; Roy,

ACPD
15, 34533–34604, 2015

1997; Goward et al., 2002; Sandholt et al., 2002; Zeng et al., 2004). In this space, land surface temperature T_s is determined by the soil thermal inertia (Lambin and Ehrlich, 1996) which is based on the assumption, that the remotely sensed surface temperatures are related to NDVI, and that NDVI is determined by land surface reflectance. The emitted heat flux from a vegetated area is lower than that from bare soil due to stomatal transpiration of the vegetation and lower thermal inertia within the vegetation (Lambin and Ehrlich, 1996; Sandholt et al., 2002). Therefore, T_s is dependent on both, the thermal inertia and the available moisture of vegetation. This relation is ideally represented in a triangle shape, when $NDVI_{surf}$ data are plotted vs. corresponding T_s data (see Fig. 3). The lower line which envelopes the triangle shaped scatter plot represents the so-called "wet edge", while the upper, negatively sloped line represents the so-called "dry edge" of any given (T_s; $NDVI_{surface}$)-data set.

Zeng et al. (2004) applied this method successfully to arid areas and showed that both linear relationships between T_s and $NDVI_{surface}$ along the dry edge (dry border) and wet edge (wet border) assured that soil moisture could be estimated from a T_s-$NDVI_{surface}$ scatter plot (Fig. 3). They defined a soil moisture index (SMI) for the T_s-$NDVI_{surface}$ space, whose value is zero along the "dry edge" and equal unity along the "wet edge". The line from point "A" to "C" in Fig. 3 represents the dry edge (dry border) of respective vegetated areas, while the line from point "B" to "C" indicates its wet edge (wet border). According to Zeng et al. (2004), the desired SMI value reads as follows:

$$\mathrm{SMI} = \frac{T_{s\ \max} - T_s}{T_{s\ \max} - T_{s\ \min}} \tag{11}$$

where $T_{s\max}$ and $T_{s\min}$ are the maximum and minimum surface temperatures in the scatter space for a given pixel, and T_s is the remotely sensed surface temperature at a given pixel for a given $NDVI_{surf}$. According to Eq. (11) SMI is the ratio of two temperature differences (for a given pixel); for instance, the value of ($T_{s\max} - T_s$) at point "D" in Fig. 3 is the temperature difference between point "E" and "D", and the value of ($T_{s\max} - T_{s\min}$) is the temperature difference between point "E" and "F".

ACPD
15, 34533–34604, 2015

$T_{s\,max}$ and $T_{s\,min}$ are defined as linear functions of $NDVI_{surface}$ and represent the enveloping lines at the dry border and wet border of the T_s – $NDVI_{surface}$ scatter space:

$$T_{s\,max} = a_1 NDVI_{surf} + b_1 \quad (12a)$$

$$T_{s\,min} = a_2 NDVI_{surf} + b_2 \quad (12b)$$

where a_1, a_2, b_1, and b_2 were obtained by linear regression of known remotely sensed data along the dry and wet edges. The SMI value for a given data point "D" ($NDVI_{surface,D}$; $T_{s,D}$) is calculated from Eq. (11) using Eqs. (12a) and (12b) to obtain $T_{s\,max,\,D}$ and $T_{s\,min,\,D}$.

2.4.5 Calibration of satellite derived SMI data

The basic concept to convert satellite derived dimensionless SMI data into the volumetric soil moisture content (θ_v) is discussed by Wagner et al. (1999) and Mallick et al. (2009). For that, specific and characteristic soil moisture values for soils of each considered land use type are needed, preferably those which may correspond to the lower and upper limits of (dimensionless) SMI data (0 and 1, see Sect. 2.4.4). As a first approximation one may assume as the lower limit for agriculturally managed land use types the volumetric soil moisture content at permanent wilting conditions ("permanent wilting point", PWP). The PWP is defined as the level at which plants will irreversible, if additional water is not provided; to avoid this the plants have to be irrigated before the PWP is reached. After heavy rain events and after irrigation events soils of vegetated land use types may reach the status of so-called (over) saturation (flooding irrigation equals to about 10–15 cm H_2O column on the soil); however, this status is only observed for about 12–24 h, after the field capacity (FC) is equilibrating. Therefore, the soil specific value at conditions of FC may be used as upper limit for the volumetric soil moisture content. Soil specific data of PWP and FC (or for flooding irrigation multiples of FC) are typically used in irrigation scheduling, calculation of plant available water, as well as water depth to be applied by irrigation (Diallo and Mariko, 2013). Both limits

ACPD
15, 34533–34604, 2015

of volumetric soil moisture content, $\theta_{v,\,min}$ at PWP and $\theta_{v,\,max}$ at FC, are usually determined by standardized laboratory measurements of water tension (pF) on undisturbed soil samples ($\theta_{v\,max}$ at pF = 1.8; $\theta_{v,\,min}$ at pF = 4.2). By knowing the corresponding bulk soil densities, volumetric soil moisture contents ($\theta_{v,\,min}$ and $\theta_{v,\,max}$) can be converted to gravimetric soil moisture contents ($\theta_{g,\,min}$ and $\theta_{g,\,max}$). With $\theta_{g,\,min}$ and $\theta_{g,\,max}$ of soil samples from each considered land use type, the corresponding SMI data (dimensionless; ranging from 0 to 1) can be transformed to data of gravimetric soil moisture content (θ_g) by:

$$\theta_g = \theta_{g,\,min} + \mathrm{SMI}(\theta_{g,\,max} - \theta_{g,\,min}) \quad (13)$$

which means SMI = 1 at $\theta_{g,\,max}$ and SMI = 0 at $\theta_{g,\,min}$.

For non-vegetated arid and hyper-arid soils (desert), the lower limit of the volumetric soil moisture content is certainly (much) lower than that at the PWP and the upper limit (at FC) may be reached at best a few hours (days) per year. Therefore, in the case of bare and desert soils, we decided to use for the lower limit a value which corresponds to "residual water" of the desiccated soil sample measured by dry mass determination as gravimetrical soil moisture after stopping each incubation experiment in the lab. Unfortunately, laboratory measurements of water tension have not been performed on the soil samples from the Tohsun oasis (desert, cotton and grape fields). Land use type specific data for $\theta_{g,\,min}$ and $\theta_{g,\,max}$ have been substituted by averages of water tension measurements (at pF = 1.8, 4.2, 6.8) performed on undisturbed soil samples taken around the Taklimakan desert during 2010 (Behrendt et al., 2014): at 8 desert sites (around the oases of Awati, Kuche, Milan, Mingfeng, Qiemo, Ruoqiang, Sache, and Waxxari), at 7 cotton field sites (within the oases of Awati, Kuche, Milan, Qiemo, Sache, Waxxari), and at 3 jujube plantation sites (within the oases of Milan, Minfeng, Qiemo); grapes and jujube both of them belong to the bushy agricultural landscape type and jujube has the similar height and distance in rows as the grapes. And they have similar water requirements and percent ground cover by their canopy. Thus, we expected the similar availability of water in the soil profile so that similar FC and PWP for grapes

ACPD
15, 34533–34604, 2015

and jujube. During July–September 2010, soil sensors (MSR® 165 data logger; see Sect. 2.2) have been buried at 2.5 cm depth at the site of Tohsun County Meteorological Station (bare soil), while in irrigated cotton, and jujube fields of the oases of Kuche and Minfeng the Frequency Domain Reflectometry (FDR) probes (ECHO-5, Decagon, USA) were used. Following the measurements of soil moisture (5 min resolution) of the latter two sites, we found, due to the applied irrigation schedules, that the lower limit of θ_g ($\theta_{g,\,min}$) was never as low as that of the PWP, i.e. regular irrigation always started long before unwanted permanent wilting conditions were reached. Instead, temporal variation of the gravimetric soil moisture content was observed between upper limits $\theta_{g,\,max,\,jujube}$ at 1.5 × FC and $\theta_{g,\,max,\,cotton}$ at 1.75 × FC (equilibrating at the time of (flooding) irrigation), θ_g at FC (equilibrating about 2.5–3.5 days after stop of irrigation), and lower limits $\theta_{g,\,min,\,jujube}$ at 0.25 × FC and $\theta_{g,\,min,\,cotton}$ at 0.5 × FC (after about 14 days, and shortly before the next irrigation cycle). We adapted these findings for the cotton and grape fields of the Tohsun oasis. Finally, we used the following $\theta_{g,\,min}$ and $\theta_{g,\,max}$ values for soil originating of the three land use types of Tohsun oasis: 0.167 and 0.586 for cotton soils, 0.086 and 0.514 for grape soils, and $\theta_{g,\,min} = \theta_{g,\,max} = 0.0028$ for desert soils.

2.4.6 Validation and calibration of satellite derived surface temperature and soil moisture data

Six Landsat images of sufficient quality were available during our observation period in 2010, namely those of 25 April (10:40 LT), 28 July (10:40 LT), 13 August (10:35 LT), 21 August (10:35 LT), 6 September (10:35 LT), and 22 September (10:35 LT). Since only one soil sensor has been buried at the Tohsun oasis during this period (2.5 cm depth; "bare soil"; Tohsun County Meteorological Station), validation of satellite derived T_s (LST) and θ_g (SMI) data of Tohsun oasis could be realized only for the "desert" land use type. For the bare soil of this site, the satellite derived surface temperature ("skin temperature") represents the actual temperature at the soil surface (0 cm depth).

ACPD
15, 34533–34604, 2015

Due to soil inertia (determined by the soil heat conductivity and capacity), any surface temperature signal needs a certain time period to propagate to deeper soil layers. From our measurements of the soil temperature profile (1, 2, 6, 10 cm depth) at the desert site of the Tohsun oasis, the time delay (surface to 2.5 cm depth) has been determined to 25 min. Consequently, for the intended validation of the satellite derived T_s (LST) data, soil temperature measurements at Tohsun County Meteorological Station (5 min resolution) have been averaged (±10 min) at a center time 25 min before the overflight of the satellite.

Behrendt et al. (unpublished data) provided the relationship between the relative humidity of soil air and the gravimetric soil water content (θ_g) based on laboratory calibration by a vapor sorption analyzer on soil samples from the Taklimakan desert. For the intended validation of satellite derived θ_g (SMI) data, the soil air relative humidity measurements at the Tohsun County Meteorological Station (5 min resolution) have been averaged (±10 min) at the respective overflight time of the satellite.

2.4.7 Two dimensional soil NO emission model

Soil NO production and soil consumption rates, as well as the resulting net NO release rates from the top soil of wheat, corn, cotton, and jujube fields of the irrigated oasis agriculture (around the Taklimakan desert) have been characterized by Behrendt et al. (2014) and Mamtimin et al. (2015), respectively. The study by Mamtimin et al. (2015) has delivered evidence for a strong contribution of biogenic soil NO emission from these managed (irrigated, fertilized) dryland soils to the local total NO_2 budget. Having (a) the net potential NO flux (F_{NO} dependent on T_s and θ_v), (b) the surface soil temperatures (T_s), (c) the volumetric soil moisture contents (θ_v), and (d) the areal distribution of the three land use types (cotton, grapes, and desert) of the Tohsun oasis available, a 2-D NO emission model was built with Arc GIS to determine the two dimensional biogenic soil NO emission source of the Tohsun oasis. This was achieved by combining information of Sect. 2.3 and 2.4, as well as the areal distribution of the field specific land use (vegetation) types of the Tohsun oasis.

ACPD
15, 34533–34604, 2015

To classify these field specific vegetation types, pre-processing the Landsat imagery and image interpretation has to be performed. To effectively record the image data, histogram equalization and edge detector techniques (Jensen, 2005) were applied during image pre-processing. By using suitable edge detecting functions, Landsat images were enhanced and boundaries between different classes were strongly highlighted for effective subsequent image interpretation. Due to the significant requirements for the different areas of interests (AOIs) of image classification, in-situ GPS data (160 points) from the field campaigns (2010) and also from previous field investigations (2006, 2008) were used. Spectral signatures of in situ data were collected by digitizing, and were consequently used to classify all pixels. For that, image spectral analysis and the mostly used supervised classification method of maximum likelihood by Jensen (2005) was performed. This procedure ensured that (a) spectral characteristics of all AOIs were used, and (b) every pixel (both, within and outside AOIs), was assessed and associated to that land-cover of which it has the highest likelihood of being a member. Then, raster data of the three most frequent land-cover types of the Tohsun oasis (cotton, grapes and desert) were implemented in the 2-D soil NO emission model to quantify the NO emissions for each location. By that, the empirical relationship of soil NO emission to its driving parameters (Eq. 2) was used to up-scale the laboratory estimates into two dimensions:

$$F_{NO}(x,y) = F_{NO}\left(\theta_{g,0}(x,y), T_{soil,0}\right)\ g\left(\theta_g(x,y)\right)\ h(T_{soil}(x,y)) \quad (14)$$

where $F_{NO}(x,y)$ is the land use type specific net potential NO flux $\theta_g(x,y)$ and $T_{soil}(x,y)$ are the land use type specific gravimetric soil moisture content and soil temperature at the center of each grid point (30 m × 30 m), $\theta_{g,0}(x,y)$ is the land use type specific, so-called optimum gravimetric soil moisture content (i.e., where the maximum NO release has been observed), and $T_{soil,0}$ is the reference temperature (here: 25 °C; identical for all land use types). The land use type specific exponential soil temperature curve $h(T_{soil}(x,y))$ and the land use type specific optimum soil moisture curve $g\left(\theta_g(x,y)\right)$ are

ACPD
15, 34533–34604, 2015

defined by Eqs. (15) and (16):

$$h(T_{\mathrm{soil}}(x,y)) = \exp\left[\frac{\ln Q_{10,\mathrm{NO}}(x,y)}{10}\left(T_{\mathrm{soil}}(x,y) - T_{\mathrm{soil},0}\right)\right] \quad (15)$$

$$g\left(\theta_{\mathrm{g}}(x,y)\right) = \left(\frac{\theta_{\mathrm{g}}(x,y)}{\theta_0(x,y)}\right)^a \exp\left[-a\left(\frac{\theta_{\mathrm{g}}(x,y)}{\theta_0(x,y)} - 1\right)\right] \quad (16)$$

Land use type specific shape factors "a" of corresponding optimum soil moisture curves were derived from laboratory drying-out incubation studies on the corresponding soil samples according to Behrendt et al. (2014). The land use type specific quantity $Q_{10,\mathrm{NO}}$ is the (logarithmic) slope of $h(T_{\mathrm{soil}})$, which was also derived from the laboratory measurements; applying two different soil temperatures, $T_{\mathrm{soil},0}$ and $T_{\mathrm{soil},1}$ ($T_{\mathrm{soil},1} - T_{\mathrm{soil},0} = 10\,\mathrm{K}$), land use type specific $Q_{10,\mathrm{NO}}$ is defined by

$$Q_{10,\mathrm{NO}} = \frac{\ln F_{\mathrm{NO}}\left(\theta_{\mathrm{g},0}, T_{\mathrm{soil},1}\right) - \ln F_{\mathrm{NO}}\left(\theta_{\mathrm{g},0}, T_{\mathrm{soil},0}\right)}{T_{\mathrm{soil},1} - T_{\mathrm{soil},0}} \quad (17)$$

In terms of data handling, an important requirement for modelling of the 2-D NO emission is the accurate description of unique identifiers. Two identifiers have been attributed to each grid point (x, y), namely (a) the geographic coordinate (x, y of the center of each grid point of the corresponding pixel), and (b) the object ID number followed by a description of (i) the land-use type, (ii) the land use type specific net potential NO flux, (iii) the land use type specific gravimetric soil moisture content, and (iv) the land use type specific soil temperature. Finally, land use type specific 2-D NO emissions were calculated for the begin, the middle and the end of the vegetation period.

2.5 Biogenic emission from soil vs. anthropogenic emission of the Tohsun oasis

The intended comparison of soil biogenic emissions in form of NO_2 and anthropogenic emissions of NO_2 confronted us with problems of (a) data availability in general, (b) in-

ACPD
15, 34533–34604, 2015

completeness of available data, (c) very different temporal scales of existing data, and (d) to find the common, reconciled temporal scale for the comparison. One would expect that anthropogenic emissions of the Tohsun oasis will peak during the winter months (due to domestic heating), while minimum emissions will prevail during summer. In contrast, biogenic emissions will exhibit the opposite temporal pattern (due to the exponential response of biogenic NO release from soils, see Sect. 2.4.7). Consequently, the common, reconciled temporal scale for the intended comparison should be at least seasonal, preferably monthly. However, calculating mean monthly land use type specific soil emissions from mean monthly data of soil temperature and soil moisture (according Eqs. 15–17) seems inappropriate due to (a) the strongly non-linear response of the soil NO release from both variables, (b) large diel variations of the surface soil temperature (e.g. 10–60 °C; desert soil; July), and (c) large weekly variations of soil moisture caused by the applied irrigation schedules. Furthermore, fertilization application (usually concurrent with irrigation) leads to fertilizer amount and time dependent amplification of NO fluxes from the agriculturally managed oases soils. Consequently, mean monthly land use type specific soil NO emissions have to be averaged from data calculated on much shorter time scales (< 1 h, in detail see Sect. 2.5.2). To make soil biogenic emissions (given in terms of mass of NO and HONO, respectively) comparable to the anthropogenic ones (which have been provided in terms of NO_2 only), respective numbers were multiplied by the respective ratios of corresponding molecular weights (M_{NO_2}/M_{NO}, M_{NO_2}/M_{HONO}).

2.5.1 Annual anthropogenic NO_2 emission of the Tohsun oasis

Tohsun oasis's anthropogenic NO_2 emissions predominantly originate from fossil fuel combustion of the energy and traffic sectors. To quantify the amount of an emitted substance from a source like fossil fuel combustion, specific emission factors have to be applied, which are expressed as the weight of the substance emitted from the mass or volume of the fuel. In P.R. China, emission factors for different economic sectors and fuel types are available, but quite variable during the last decade. Based on the avail-

ACPD
15, 34533–34604, 2015

able sparsely statistical data, the most frequently used fuel types in Tohsun are coal, coke, crude oil, natural gas, diesel, and gasoline. Thus, we used those NO_x emission factors which are widely used in P.R. China (Hao et al., 2002; Zhang et al., 2009; Shi et al., 2014), and which are based on the following equation:

$$E^N_{i,j(k),f}(t) = \left(1 - P^N_{i,j(k),f}(t)\right) \cdot K^N_{i,j(k),f}(t) \cdot F_{i,j(k),f}(t) \quad (18)$$

Here E^N (in kg) is the mass of emitted NO_x (calculated as NO_2), P^N is the dimensionless removal efficiency of the emission reduction technology (if applied); K^N (in kg t^{-1}) is the emission factor (mass of emitted NO_x per mass of fuel, weighted as NO_2); F (in t) is the fuel consumption; the subscript "i" represents any autonomous region or province of P.R. China (here: Turpan County); the subscript "$j(k)$" is the emission source category in the economic sector "k"; the subscript "f" is the fuel type, and "t" is the time (year). It should be noted that information on Tohsun County's fuel consumption is only available on an annual basis; however, coal is the dominating fuel type of energy consumption (65 % of total; Pu, 2009, 2011). Tohsun's heating system changed in 2007, the former inefficient central coal fired boiler was shut down and replaced by decentral heating systems. Most of the boilers of the central heating facilities were based on "low NO_2 burner technologies", which means that the potential coefficient of emission-reduction for coal-fired thermal power is equal to 0.67 (Zhou, 2006; Mao et al., 2012). For calculation of the emission factor of electric power, we multiplied the uncontrolled emission factors by the new removal efficiency coefficient. The NO_2 emission factors used in this study are summarized in Table 1.

2.5.2 Specific land use type soil temperature, gravimetric soil moisture content, and fertilizer factor

Due to the very low soil temperature before and after the growing season (see Fig. 1b), most of the soil surface is expected to be frozen and F_{NO} from any soils of the Tohsun oasis can be neglected. Thus, mean monthly soil NO emissions are only calculated for

ACPD
15, 34533–34604, 2015

the period April to September. Calculation of mean monthly land use type NO emissions (according Eqs. 15–17) needs temporally high resolution (< 1 h) data sets of soil temperature and gravimetric soil moisture content for grape, cotton, and desert soils. In-situ measurements of both quantities (5 min resolution) at the Tohsun oasis have been performed only for the land use type "desert", and only for the period 1 July to 30 September 2010 (see Sect. 2.2). During the same period, soil temperature and soil moisture (at 2.5 cm depth) have also been measured for the land use types "cotton fields" and "jujube fields" (which substitute Tohsun oasis' grape fields; see Sect. 2.4.5) at the Taklimakan oases Kuche (41.5360° N, 82.8546° E) and Minfeng (37.0534° N; 82.0760° E), respectively. For the spatial adjustment and temporal scaling of the three soil temperature data sets ("desert", "cotton fields", "grape fields"), the corresponding Landsat satellite derived surface temperatures of 25 April, 28 July, 13 and 21 August, and 6 and 22 September 2010 (approx. 10:45 LT) have been used (see below).

For the entire growing season (April–September 2010) a constant value of the gravimetric soil moisture content (0.0028) has been chosen for Tohsun oasis' desert soils. Following the observations at the oases of Kuche and Minfeng, a temporally constant irrigation schedule, starting at 1 April and repeated every 2 weeks, as well as corresponding "drying-out" shape functions have been adapted for the land use types "grape soils" and "cotton soils" of the Tohsun oasis.

To maintain the productivity of the grape and cotton fields of the Taklimakan oases, the soils regularly receive considerable N-containing fertilizer amounts (see Sect. 2.1). The impact of the fertilizer application on the NO-fluxes from arable soils of the Taklimakan oases was recently investigated by Fechner (2014) using the laboratory dynamic chamber system described by Behrendt et al. (2014). Dependent on the applied fertilizer amount (FA), NO-fluxes from all soil samples increased considerably, immediately after fertilizer application, which was accomplished by dissolving the mineral fertilizer in that amount of water which was used to wet the soil samples (just to mirror the fertilization procedures of the Taklimakan oases). The impact of fertilization is twofold, (a) it strongly amplifies the net release (net potential flux) of NO over the entire

ACPD
15, 34533–34604, 2015

range of gravimetric soil moisture, and (b) there is an only moderate amplification of the net NO release (net NO potential flux) with soil temperature. The fertilizer effect may be considered by the multiplicative, FA-dependent, and dimensionless "fertilizer factor (FF)" applied to the standard net release $J_{NO}(\theta_{g,0},T_{soil,0})$ in Eq. (2), and as the FA-dependent, and the dimensionless "Q_{10} factor ($Q_{10}F$)" also multiplicatively applied to Q_{10} (the logarithmic slope of the exponential soil temperature curve $h(T_{soil})$). Given fertilization amounts FA = 100, 200, 300, and 400 kg (N) ha^{-1} result in FF = 142, 179, 205, and 226, and $Q_{10}F$ = 1.21, 1.24, 1.25, and 1.26, respectively.

2.5.3 Data assimilation

Unfortunately, data of fossil fuel consumption from the different economic sectors of Tohsun County (see Sect. 2.2) are only available on an annual basis. For down-scaling to mean monthly values, the corresponding mean monthly percentage of NO_2 of Urumqi (140 km NNW of Tohsun) has been used. Based on the data from Mamtimin et al. (2011) the monthly percentage of NO_2 for Tohsun adapted from Urumqi and expressed as following: 0.148, 0.157, 0.125, 0.069, 0.041, 0.035, 0.031, 0.046, 0.051, 0.066, 0.099, and 0.132 for January to December, respectively.

For temporal up-scaling of the Landsat satellite derived land use type specific surface temperature data, corresponding values for "desert", "cotton fields", "grape fields" have been fitted by 3rd order polynomials with respect to the day of year (DOY) 2010 (see Fig. 4). As a result, land surface temperatures (at 10:45 LT; i.e. satellite overflight) for the Tohsun oasis' land use types can be calculated for every individual day between 1 April and 30 September 2010. Soil temperature measurements (5 min) for the land use types "desert", "cotton fields", and "grape fields" are available only for the period 1 July to 30 September 2010. To obtain data sets suitable for the entire considered time period (April–September 2010), the following approach has been chosen. Each data point of a particular day has been normalized by the mean value observed at 10:45 LT (± 15 min), the time of the Landsat satellite overflight. A data set of mean diel variation (30 min) of these normalized soil temperatures (5 min) has been created by averaging

ACPD
15, 34533–34604, 2015

all respective data between 1 July–30 September, constituting the representative diel variation of the (normalized) soil temperature of the respective land use type valid for the entire growing period (see Fig. 5). The diel variation of soil temperatures of the land use types "desert", "cotton fields", and "grape fields" for every day of the growing period 2010 are obtained by multiplying the normalized soil temperature data (Fig. 4) with the respective land surface temperature of this particular day (see above).

Since there is no official information on Tohsun oasis' irrigation available, irrigation schedules and "drying-out" shape functions observed at Minfeng and Kuche oases have been adapted for the land use types "grape fields" and "cotton fields" of the Tohsun oasis, respectively (see Fig. 6). Gravimetric soil moisture contents before the first irrigation event have been chosen as 0.086 ("grape soils") and 0.167 ("cotton soils"), which correspond to mean gravimetric soil moisture contents at conditions of 0.25 × FC and 0.5 × FC, respectively. The maximum gravimetric soil moisture contents (after irrigation) have been set to 0.514 ("grape soils") and 0.586 ("cotton soils"), which correspond to mean gravimetric soil moisture contents at conditions of 1.5 × FC and 1.75 × FC, respectively (as observed on a total of 12 Taklimakan oases; see Sect. 2.4.5).

There is also no official precise information on Tohsun oasis' fertilizer rates and fertilization schedules. In Xinjiang as well as in Tohsun, the rate of fertilizer was applied according to the local farming regime, which varied greatly among the different farms (Chen et al., 2008). Therefore, for consideration of the fertilizer effect (i.e. the amplification of the net NO fluxes through fertilizer application), we followed the recommendations of the local agricultural administration (personal information, 2010) and our personal communication with farms (2010). The first fertilization ("base fertilizer event") usually occurs in early April, applying $200 \pm 50\,\mathrm{kg\,(N)\,ha^{-1}}$ to grape fields, and $310 \pm 40\,\mathrm{kg\,(N)\,ha^{-1}}$ to cotton fields.

During the rest of the growing period four more fertilizing events follow, namely at the end of May, mid of June, end of July, and beginning of August, with 20–35 % of the "base fertilizer event" amount in May and June, and 50–60 % in July and August. It is known, that the fertilizer effect on the emission of N-containing gases is temporally

ACPD
15, 34533–34604, 2015

declining after a fertilization event (Chen et al., 2011). This decline has been considered by the time-dependent, exponential decays of FF and $Q_{10}F$, starting with given, FA-dependent FF- and $Q_{10}F$-values (s. Sect. 2.5.2) six hours after the respective fertilization events, and ending with FF = $Q_{10}F$ = 1 after 14 days. The latter event accounts for the common practice at the Taklimakan's oases that agriculturally managed fields receive fertilizer concurrently with (or even dissolved in) irrigation waters; the delay of six hours (after each fertilization event) accounts for equilibrating unavoidable disturbances during fertilization and/or irrigation events. The seasonal course of FF- and $Q_{10}F$-values resulting from the described data assimilation is shown in Fig. 7.

The recent findings of Oswald et al. (2013), namely that large amounts of gaseous nitrous acid (HONO) are concurrently emitted along with NO, have been considered for the monthly estimation of biogenic emissions of the Tohsun oasis. Oswald et al. (2013) have investigated a total of 17 soil samples which have been taken from a variety of natural and agriculturally managed soils around the globe. Fortunately, five of these samples (no. S13–S17 in Oswald et al., 2013) were cotton, jujube, and desert soils of the Taklimakan region, most of them of similar properties to those used for this study. Monthly land use type specific contributions of HONO emission for the Tohsun oasis during the growing period 2010 were estimated by multiplying the corresponding NO emissions with the mean, land use type specific factors (0.8 for grape and desert soils, and 1.6 for cotton soils); these were calculated from individual values provided by Oswald et al. (2013).

2.6 NO_2 emission from the Tohsun oasis: satellite derived vs. laboratory derived (up-scaled) data

Satellite retrieved tropospheric NO_2 columns over the Tohsun oasis provide a daily measure for the vertically integrated NO_2 concentration (during the time of overflight, around 13:00 LT). To calculate the satellite derived top-down NO_2 emissions the integrated OMI satellite monthly means were used. Only a few assumptions are necessary to derive NO_2 fluxes from this data: (1) these NO_2 molecules originate exclusively

ACPD
15, 34533–34604, 2015

from NO_2 emissions (anthropogenic + biogenic) from the area of the Toshun oasis, (2) the depletion of NO_2 in the Atmospheric Boundary Layer is primarily due to the reaction of NO_2 with the hydroxyl radical OH (leading to the formation of gaseous nitric acid, HNO_3) and the characteristic time (lifetime) of the depletion is approximately known. It has been e.g. investigated by Beirle et al. (2011) and can be estimated to about τ_{NO_2} = 4 h for low and mid-latitudes, particularly for the dryland cities of Isfahan (32.6° N) and Riyadh (24.6° N).

To account for any background NO_2 from upwind (desert) areas, the representative VCD_{NO_2} observed over the Taklimakan desert was subtracted from the VCD_{NO_2} observed over the Tohsun area. NO_2 emissions from the Tohsun oasis (ng m^{-2} s^{-1}, in terms of NO_2) can be calculated by dividing the integrated VCD_{NO_2} data by the characteristic lifetime of NO_2. The corresponding results represent the total NO_2 emission (i.e. from anthropogenic and biogenic sources) from the area of the Tohsun oasis at the time of OMI satellite overflight (and a few hours before).

Bottom-up fluxes are derived from the net potential NO fluxes (laboratory incubation, s. Sect. 2.3) spatially up-scaled to the Tohsun oasis area taking into account the corresponding soil temperatures (T_{soil}), gravimetric soil moisture contents (θ_g), and fertilizer factors (FF, $Q_{10}F$), see Sect. 2.5.3. To make the up-scaled (soil biogenic) emissions (given in terms of mass of NO) comparable to the satellite derived, correction factors according to the ratio of the corresponding molecular weights (M_{NO_2}/M_{NO}) were applied.

Here it is important to note that the tropospheric VCDs derived from satellite measurements can be systematically affected by the a-priori assumptions needed for the calculation of the air mass factor AMF (reflecting the satellite sensitivity for tropospheric NO_2), such as cloud fraction, cloud pressure, surface albedo, and trace gas profile (Boersma et al., 2007, 2011). Fortunately, the region of Tohsun County provides relatively favourable conditions for accurate calculation of tropospheric AMFs, since the desert region is typically only little affected by clouds, aerosols; also lightning activity is rather weak. The AMF for OMI DOMINO v2.0 has been calculated using TM4 model

ACPD
15, 34533–34604, 2015

NO_2 profiles with a longitude–latitude resolution of 3° × 2°, a surface reflectance climatology (0.5° × 0.5°), and cloud information (Boersma et al., 2011). To test whether the assumed surface albedo is appropriate for the Toshun oasis, we examined the OMI surface reflectance climatology for the study area, and compared it with the high resolution MODIS surface reflectance product (0.05° × 0.05°, MOD43B). We used the MODIS albedo products from channel 3 (at 459–479 nm) because this channel is close to the spectral window (405–465 nm) used for the OMI retrieval. According to Kleipool et al. (2008) the surface albedo difference between 470 nm (center of MODIS channel) and 440 nm (OMI surface reflectance climatology) is very small for land surfaces. The TM4 model NO_2 profile for oasis (over grapes field) and desert area (400 km away from the oasis, in Taklimakan desert 85.5129° E, 40.0669° N) were investigated as area of emission source and background area, respectively.

3 Results and discussion

3.1 Laboratory derived net potential NO fluxes

Results of the laboratory derived net potential NO fluxes (F_{NO}) from soils of the desert and the irrigated and fertilized cotton and grape fields of are shown in Fig. 8. In the Tohsun oasis the mean net potential NO flux of cotton was highest at laboratory incubation temperature of 25 °C, with a peak mean net potential NO flux of 125 ng m^{-2} s^{-1} followed by grapes (41 ng m^{-2} s^{-1}) and desert (9 ng m^{-2} s^{-1}), respectively. Common to the net potential NO fluxes from the major land use types of the Tohsun oasis is the exponential response to soil temperature (due to strong enzymatic activites associated with microbial soil NO production processes). During the growing period (April–September), soil temperatures of > 45 °C are easily reached for the soils of the Tohsun oasis, particularly for the desert soils (see Sect. 3.3.). At T_{soil} = 50 °C, the maximum net potential NO fluxes of 834 (cotton soils), 249 (grape soils), and 99 ng m^{-2} s^{-1} (desert soils) are reached at an optimum gravimetric soil moisture content ($\theta_{g,\,opt}$) of 0.021,

ACPD
15, 34533–34604, 2015

0.146, and 0.0158, respectively. These $\theta_{g,\,opt}$-values, particularly those of the cotton and desert soils, are much lower than those of natural and agriculturally used soils of temperate latitudes (> 0.25, c.f. Oswald et al., 2013; Behrendt et al., 2014).

Remarkably, a significant net potential NO fluxes from desert soil only occurs if θ_g is higher than 0.01 and less than 0.03. Since the observed θ_g-value of the Tohsun desert soils is 0.0028 (s. Sect. 2.5.2), no significant biogenic NO emissions are expected from there. As stated in Sect. 2.5.3, the chosen irrigation schedules of cotton and grape fields resulted in certain ranges of gravimetric soil moisture contents (oriented on the field capacity of the respective soils). Immediately after each irrigation event θ_g-values of 0.514 (grape soils) and 0.586 (cotton soils) occur; consequently, there will be no significant biogenic NO emissions at this stage. After 14 days (just before the next irrigation event), θ_g-values of 0.086 (grape soils) and 0.167 (cotton soils) are found; consequently, regarding the results in Fig. 8, maximum biogenic NO emissions from grape soils have to be expected to the end of the 14 day irrigation period ($\theta_{g,\,opt}$ = 0.146), while at that time biogenic NO emissions from cotton soils will be (even at T_{soil} = 50 °C) less than 10 ng m^{-2} s^{-1}, since then the θ_g value for cotton soils (0.167) is far above the corresponding optimum value ($\theta_{g,\,opt}$ = 0.021). This means, that despite the overwhelming potential of cotton soils to dominate the biogenic NO emissions of the Tohsun oasis (s. Fig. 8), their net actual contribution is almost negligible over the full 14 days irrigation cycles (see Sect. 3.6). Here it should be noted that for other oases (with other irrigation cycles) the contribution cotton soils might be much larger.

3.2 Analysis of the T_s–NDVI$_{surf}$ scatter space

The soil Moisture Index (SMI) was calculated using the parameters a_1, a_2, b_1, and b_2 which are obtained from linear regression analysis along the dry and wet borders of the triangular T_s–NDVI$_{surface}$ scatter spaces (s. Sect. 2.4.4, Fig. 2).

To determine the dry and wet edges, the Landsat images of 25 April (begin of the vegetation period), 28 July, 13 and 21 August (middle of the vegetation period), and 6 and 22 September (end of the vegetation period) were used. Figure 9 clearly shows

ACPD
15, 34533–34604, 2015

the triangular shape of the scatter plot between $NDVI_{surface}$ (horizontal axis) and T_s (vertical axis). The interpretation of the triangular shape is (Zeng et al., 2004): the more vegetated an area (the higher the $NDVI_{surface}$), the lower the surface temperature. Thus, for a given $NDVI_{surface}$, low T_s values correspond to high amounts of soil moisture (high amounts of SMI). The linear relationship between T_s and $NDVI_{surface}$ is in any case statistically significant ($R^2 > 0.7$; s. Fig. 9).

3.3 Land cover classification

The land-cover classification of the Tohsun oasis has been also derived from Landsat images (Sect. 2.4.6). The areal distribution of land-cover is shown in Fig. 10. Five land-cover types, shown in a land-cover raster map (30 m × 30 m), were identified, namely cotton fields, grape fields, other vegetation, buildings/residential areas, and desert. Based on these results, the dominant land cover types were cotton and grapes, representing 10.2 % (150 km^2) and 6 % (80 km^2) of the investigated domain, building/residential area 2.8 % (42 km^2), other vegetation 4.8 % (72 km^2), desert 75 % (1117 km^2), unidentified 1.2 % (18 km^2).

3.4 Validation of the satellite derived soil temperature and soil moisture content data

As mentioned in Sect. 2.4.6, the validation of the satellite derived T_s (LST) and θ_v (SMI) data of the Tohsun oasis could be performed only for one land use type ("desert"), since only one soil sensor has been buried at the Tohsun oasis in bare soil at the Tohsun County Meteorological Station (see Fig. 10) during July–September 2010. Satellite derived land surface temperature data (LST) and gravimetric soil moisture content data (θ_g, derived from SMI) and the results of the corresponding in situ data are shown in Fig. 11a and b for the five Landsat images (28 July, 13 and 21 August, 6 and 22 September 2010), which were available during the time period of our in situ measurements (July–September 2010).

ACPD
15, 34533–34604, 2015

There is very good agreement of the satellite and in situ surface temperature data as corresponding statistical tests indicated no significant difference between the two data sets ($P < 0.01$). In case of gravimetric soil moisture content, there is also no significant difference between satellite derived and in situ measured data considering the given errors of both data sets. However, it has to be noted, that this validation has been performed for a desert-like soil with an extremely low gravimetric soil water content (< 0.004).

3.5 Variation of the soil temperature and soil moisture content at oasis scale

The development of the Geoscience General Tool Package (GGTP, s. Sect. 2.4) and its application to Landsat images allowed us to present maps of the 2-D distribution of Tohsun oasis' land surface temperature for the begin, the middle, and the end of the 2010 vegetation period, i.e., on 25 April, 28 July, 13 and 21 August; 6 and 22 September, respectively. Corresponding patterns of Tohsun oasis' land surface temperature are shown in Fig. 12. Cultivated parts of the oasis are sharply separated from the surrounding desert, related land surface temperature differences exceed 10 °C for all growth stages. However, significant temperature differences were also observed between cotton and grape fields, particularly in July; here, land surface temperatures were 35–55 °C in grape fields, and 25–50 °C in the cotton fields. Lower skin temperatures of the cotton fields were due to (a) effective shading of the soil by the fully developed cotton canopy which is considerably more dense than that of the grapes, and (b) transpiration of the cotton leaves which are known for highest transpiration rates.

The corresponding patterns of Tohsun oasis' gravimetric soil moisture content, derived from satellite derived T_s and $NDIV_{surface}$ information, calibrated by laboratory measurements of soil moisture at FC, PWP, and residual water conditions (s. Sect. 2.4.5), are shown in Fig. 13. In all cases, gravimetric soil moisture contents of the cultivated parts of Tohsun oasis (0.085–0.33) were significantly higher than those of the surrounding desert, (0.0028). With respect to the growth stage of Tohsun oasis' vegetation, lowest soil moisture contents (0.085–0.18) have been observed at the beginning of the

ACPD
15, 34533–34604, 2015

growing period (April); highest values have been identified in July and August (0.33). Throughout the growing period there was less difference between the gravimetric soil moisture content in the cotton and the grape fields. Particularly in July, the grapes fields seem to have stored similar amounts of available water to the cotton fields: corresponding θ_g–values of cotton fields were between 0.167–0.33, and between 0.085–0.25 for the grape fields.

3.6 2-D distributions of biogenic soil NO emissions

As mentioned above in Sect. 2.4.7, the land use type specific NO emissions from cotton, grape, and desert soils were calculated from the corresponding laboratory derived net potential NO fluxes and from satellite derived land use type specific soil moisture and surface temperature. In the framework of the 2-D soil NO emission model, the data were assigned to each individual NO source unit (fields) of cotton soils (3524 polygons), grape soils (1874 polygons), and desert desert (1419 polygons). The land use type specific NO emissions for the beginning, the middle, and the end of the 2010 vegetation period, i.e., on 25 April, 28 July, 13 and 21 August, 6 and 22 September 2010, are shown in Fig. 14. In the cotton fields a mean NO emission of 0.007, 0.02, 0.013, 0.0154, 0.009 and 0.008 $\mathrm{ng\,m^{-2}\,s^{-1}}$ was observed in 25 April, 28 July, 13 August, 22 August, 6 September and 22 September, while the mean NO emissions in grape fields are 20, 85, 68, 39, 36, 26 $\mathrm{ng\,m^{-2}\,s^{-1}}$, respectively. Although the grape fields of the Tohsun oasis receive less fertilizer than the cotton soils (see Sect. 2.1), highest mean NO emissions from grape soils are most likely due to the much higher soil temperatures, since the grapes' canopy provides only marginal shade to the soil. For the observation in April, the maximum NO emission (28 $\mathrm{ng\,m^{-2}\,s^{-1}}$,) was estimated from the grapes fields. With increasing soil temperatures, i.e. in the middle (July and August) and at end (September) of the growing period, maximum emissions (345, 278, 42 $\mathrm{ng\,m^{-2}\,s^{-1}}$) have always been obtained for the grape fields.

As results from this study, the net potential emission of NO from the soil is largely controlled by soil moisture, temperature, and fertilizer application. Under conditions of

ACPD
15, 34533–34604, 2015

our simulation (14 days irrigation cycles), the low optimum soil moisture of cotton is not reached. As a consequence, NO emissions from cotton soils can be neglected if compared with emissions from grape soils, even though the net potential emission of cotton soils is more than three times higher than for grape soils. It should, however, be emphasized that just small changes in low optimum soil moisture may cause higher NO emission than estimated. Since net potential NO flux of cotton may result in an increased emission for a few hours before the next irrigation event.

Summing up the 2010 NO emission rates for the entire oasis, the corresponding totals (observations of April + July + August + September) are 1328 $g\,s^{-1}$. The corresponding 2010 "seasonal" data are 98 (25 April), 408 (28 July), 330 (13 August), 189 (21 August), 173 (6 September) and 127 $g\,s^{-1}$ (22 September), for oasis soils (grapes + cotton), while the corresponding data for "desert soils" are assumed to be independent of "season" (3 ± 1 $g\,s^{-1}$). The six 2-D distributions of Tohsun oasis' biogenic NO emission rates shown in Fig. 14 are not more than "snapshots" ("taken" at 10:45 LT of the six selected days). Thus, for any comparison of soil biogenic emissions with anthropogenic emissions and satellite observations longer time scales (preferably monthly means) for the biogenic emissions have to be considered (see Sect. 2.5). The corresponding results are presented in the next section.

3.7 Comparison of biogenic soil and anthropogenic NO_2 emission

3.7.1 Annual anthropogenic NO_2 emission of the Tohsun oasis

Annual NO_2 emissions of the Tohsun oasis have been determined from published information on annual consumption of different fossil fuel types and related NO_2 emission factors which are widely used in P.R. China (s. Sect. 2.5.1). Results of nitrogen emission per fuel type (in terms of NO_2) for 2010 are shown in Fig. 15. In Tohsun, like other parts of China, coal combustion is the largest contributor to NO_2 emissions and is accounting for approx. 58 % (5040 t) of the NO_2 emission inventory. As the second largest contributor, coke combustion contributed about 10 %.

ACPD
15, 34533–34604, 2015

3.7.2 Land use type specific net NO fluxes based on assimilated data of soil temperature, soil moisture content, and enhancement by fertilizer application

Biogenic net NO fluxes (in ng m^{-2} s^{-1}, in terms of NO) from the three land use types of the Tohsun oasis have been calculated by Eq. (2) from assimilated data sets of soil temperature, gravimetric soil moisture content, and the enhancement of biogenic net NO fluxes caused by regular fertilizer application (s. Sect. 2.5.3). The 3-D graphs of the seasonal variation of the mean diel soil temperature are presented in Fig. 16 for desert, grape, and cotton soils of the Tohsun oasis. As expected, soil temperature in desert soils exhibits the largest variation on both, diel and seasonal scales, while, due to the shading by the considerably dense canopy of cotton plants, the corresponding variations of the soil temperature in cotton fields are smallest. The seasonal variation of the diel variation of the biogenic net NO flux from soils of the land use types "grape soils" and "cotton soils" are shown in Fig. 17. Results of the biogenic net NO flux from desert soils are not shown. Despite very high values of the soil temperature, the net NO fluxes from Tohsun oasis' desert soils are ($\ll 1\,ng\,m^{-2}\,s^{-1}$) due to the extremely low gravimetric soil water content assumed for the Tohsun's desert soils ($\theta_{g,\,desert}$ = 0.0028).

The biogenic net NO fluxes from grape soils are dominating by far, and exceed those from cotton soils on average by a factor of $1 - 2 \times 10^3$. In both soils, the seasonal and diel variations of the net NO fluxes clearly mirror those of the corresponding soil temperature. On the seasonal scale, there is striking evidence for the impact of the chosen irrigation schedules particularly on the net NO fluxes from cotton soils (through the assumed regular 2 weekly variation of the corresponding gravimetric soil moisture content). Immediately after (flooding) irrigation, soils might be water-logged which prevents any diffusion of gases out of the soil; but even after evaporation of the surface waters, the chosen "drying-out" curves (s. Fig. 7) prescribe θ_g-values of 0.514 ("grape soils") and 0.586 ("cotton soils") which are well above the corresponding values at field ca-

ACPD
15, 34533–34604, 2015

pacity conditions. There, soil diffusivity as well as soil microbial processes are severely suppressed (c.f. Skopp et al., 1990). This is clearly reflected in the results of laboratory incubations (s. Fig. 9), where the corresponding net potential NO fluxes are close to zero for $\theta_g > 0.4$. Approaching the end of the chosen 14 day irrigation period, θ_g-values reach 0.086 and 0.167 for grape soils and cotton soils, respectively. Then, the soil diffusivity is no longer limited in both soils, but soil microbial processes in cotton soils are still far from their maximum activity ($\theta_{g,\,opt} = 0.021$), while soil microbial processes in grape soils have even passed their maximum activity ($\theta_{g,\,opt} = 0.146$). That is why biogenic net NO fluxes from grape soils of the Tohsun oasis are dominating those from cotton soils. Furthermore, the impact on net NO emission by fertilizer application on 1 April (DOY 91), 27 May (DOY 147), 10 June (DOY 161), 22 July (DOY 203), and 5 August (DOY 217, s. Fig. 7) amplifies the already higher net NO fluxes from grape fields.

3.7.3 Monthly NO_2 emissions of the Tohsun oasis: soil biogenic vs. anthropogenic contributions

Given the areal contributions of the three land use types of the Tohsun oasis (1117, 80, and 150 km^2 for desert, grape, and cotton soils), the corresponding monthly biogenic NO and HONO emissions have been calculated (s. Sect. 2.5 and 2.6). Monthly anthropogenic emissions (given in terms of mass of NO_2) have been calculated from Tohsun County's annual NO_x emission data, which were down-scaled by appropriate mean monthly percentages (s. Sect. 2.5.1) and these results are shown in Fig. 18.

On annual basis (not shown), anthropogenic sources contribute by 81.4 %, biogenic sources by 18.6 % (10.3 % NO, 8.3 % HONO) to Tohsun oasis' total emissions (7246 t, in terms of NO_2) of reactive nitrogen in 2010. However, if only the growing period (April–September) is considered, where 40 % (2884 t) of Toshun oasis' total annual emissions occur, the anthropogenic emissions contribute about 53.2 %, and biogenic sources about 46.8 % (26.0 % NO, 20.8 % HONO). Despite the chosen regular 2 weekly variation of the gravimetric soil moisture content for grape and cotton soils (s. Fig. 6) and

ACPD
15, 34533–34604, 2015

the prescribed fertilization scheme (s. Fig. 7), soil biogenic emissions seem to be, at monthly scales, under primary control of the soil temperature; indeed, the seasonal variation of the total soil biogenic emissions mirrors exactly that of the soil temperature (s. Fig. 16). Particularly during July, when soil temperatures are highest (s. Fig. 16), both, soil NO emissions (227 t) and soil HONO emissions (182 t) exceed the corresponding anthropogenic emissions (147 t); during June, July and August, total biogenic emissions (NO and HONO) exceed the anthropogenic emissions by factors of 1.8, 2.8, and 1.5, respectively. Consequently, biogenic soil emissions of NO and HONO during the growing period are certainly much more important contributors to the regional NO_2 budget (hence to regional photochemistry) than thought before.

3.8 Spatio-temporal variation of the tropospheric VCD_{NO_2} measured from satellite

OMI satellite data of tropospheric NO_2 were chosen because of their smaller pixel size (13 km × 24 km in nadir) compared to data from SCIAMACHY (60 km × 30 km), or GOME (320 km × 40 km). OMI data also provides daily global coverage (Boersma et al., 2007). For our study we used the OMI monthly mean tropospheric NO_2 data, which is calculated on the basis of the results of daily OMI overflights (around noon), and is provided by TEMIS (Tropospheric Emission Monitoring Internet Service, European Space Agency (ESA); http://www.temis.nl/). The OMI monthly mean tropospheric NO_2 data product was averaged on a 0.125° × 0.125° grid, and has been retrieved for cloud fractions < 20 %.

Figure 19 shows the seasonal means for spring, summer, autumn and winter (from 2006 to 2010) of the tropospheric NO_2 VCD around the Tohsun oasis. For all seasons enhanced values are found over the area of the Tohsun oasis (compared to the surrounding desert). Similar or even stronger enhancements are also found for other regions, which are dominated by anthropogenic activities, especially Urumqi. To investigate the seasonal cycle in more detail, time series of monthly means are calculated

ACPD
15, 34533–34604, 2015

for four selected areas (see Fig. 20): agriculturally used area (A: study area), mixed land use area (B: agricultural and urban), large urban area (C), and desert (D).

The seasonal variation of the tropospheric VCD_{NO_2} for the different land use types is shown in Fig. 21. The comparison among the four land use types indicates that the large urban area Urumqi (Mamtimin et al., 2011) shows the highest NO_2 VCDs, followed by Tohsun, Tohsun and Turpan area, and desert. From the seasonal cycles, clear indications on the relative contributions from fossil fuel combustion and soil emissions can be drawn: Over Urumqi clear maxima are found during winter indicating the dominating contribution from fossil fuel combustion. In contrast, over desert, a maximum is found during summer, which is caused by enhanced soil emissions during summer. Over the oases (B and C) a first maximum is found in winter related to enhanced fossil fuel combustion during the heating period. However, a secondary maximum is found in summer, which indicates that during summer soil emissions also substantially contribute to the total NO_x emissions.

3.9 NO_2 emissions from Tohsun oasis: satellite derived top down emissions vs. laboratory derived bottom-up emissions

In this section we investigate the satellite derived top-down NO_2 emissions of the Tohsun oasis and compare these with the bottom-up emission estimates (anthropogenic and/or biogenic). As already mentioned in section 2.6, we subtracted the background values determined over the desert from the NO_2 VCDs over the oasis. The seasonal cycles of the top-down (satellite derived) and bottom-up emissions (anthropogenic and biogenic) over the Tohsun oasis are shown in Fig. 22.

The sesonal cycle of the bottom-up emissions (for both anthropogenic and biogenic sources) shows a first maximum in winter and a second maximum in summer; the same seasonal cycle is also found in the top-down emissions derived from the satellite observations. Interstingly, the second maximum in summer is only found, if the soil emissions are taken into account. This finding confirms that during summer soil emissions play an important (if not the dominant role) over the Toshun oasis.

ACPD
15, 34533–34604, 2015

Especially the good quantitative agreement was unexpected and might be partly caused by the cancellation of different systematic errors. Especially for the top down emissions from the satellite observations two important assumptions have to be made, which affect the emission estimates:

First an air mass factor has to be calculated for the conversion of the retrieved slant column densities into the vertical column densities. Here particularly assumptions on the trace gas profile and the surface albedo have to be made. For NO_2 vertical profiles from a global model (TM4, see Sect. 2.6) with a rather coarse spatial resolution are used. Thus it can be expected that the true NO_2 profile over the Toshun oasis is probably located closer to the surface than the profile from the global model. As a consequence, the true air mass factor is probably smaller than the one used in the OMI retrieval, and thus the NO_2 VCD from the operational product probably underestimates the true tropospheric NO_2 VCD. In contrast, the surface albedo used in the operational product is very similar to those from other data sets (MODIS and MERIS). Here it is interesting to note that the spatial patterns of the surface albedo and the tropospheric NO_2 VCD show no similarities.

Second, the assumed lifetime might differ from the true atmospheric lifetime. Here we assumed a constant lifetime of 4 h over the whole year. While this value is probably appropriate for summer, it is probably too small for winter. Thus the top-down emission estimates in winter probably overestimate the true emissions.

Also for the bottom-up estimates uncertainties exist (see also Sect. 3.1 and 3.6). In particular the estimated emissions from cotton soils depend critically on the irrigation cycles (see Sect. 3.1). Because of these uncertainties, the good quantitative agreement between top-down and bottom-up emission estimates should be treated with caution.

ACPD
15, 34533–34604, 2015

4 Summary

This study is focussing on the investigation and quantification of biogenic NO emission from agriculturally managed soils of the Tohsun oasis (i.e. from soils of grape and cotton cultivation). Biogenic emissions of nitrous acid (HONO, concurrently emitted with NO) are also estimated using scaling factors applied to the modelled NO emissions. We applied the following methodology: firstly, the Geoscience General Tool Package (GGTP) has been developed to obtain soil temperature, soil moisture and biogenic soil NO emission at oasis scale. Secondly, mean diel variation of the normalized soil temperatures, seasonal variation of the gravimetric soil moisture content and fertilizer factors (FF, $Q_{10}F$) were assimilated to calculate the mean monthly land use type specific soil NO emissions during the growing period by suitable assimilation techniques.Thirdly, data of anthropogenic NO_2 emissions (down-scaled from annual to monthly values) are estimated and compared to the mean monthly soil biogenic NO_2 emissions (NO+HONO). Fourth, top-down emissions over the Tohsun oasis have been derived from satellite observations.

The importance of soil biogenic emissions to the regional tropospheric NO_2 budget has been demonstrated by the comparison between monthly biogenic soil emissions of NO_2 (and HONO) and corresponding anthropogenic NO_2 emissions; during the growing period, particularly between July to September biogenic emissions are (at least) equal until twofold of the related anthropogenic sources. From the three considered land use types of the Tohsun oasis (desert, grape, and cotton soils) grape soils (fertilized and irrigated) are the main summertime contributor to the biogenic NO_2 (NO and HONO) emissions of the oasis, while emissions from cotton soils can be almost neglected for the case of the Toshun oasis (particularly because of the specific irrigation cycle). Here it should be noted that the contribution from cotton might be by far higher for other oases. During winter, the soils are frozen and the corresponding emissions are negligible; thus during that season anthropogenic emissions by far dominate the total NO_x emissions of the Toshun oasis. As a consequence of both anthropogenic and nat-

ACPD
15, 34533–34604, 2015

ural contributions, a seasonal cycle of the total emissions with two peaks (a strong peak in winter and a secondary peak in summer) is derived. This seasonal cycle is found in both the top-down and bottom-up emission estimates. Also good quantitative agreement between both techniques was found. These results provide strong evidence that biogenic emissions from soils of managed drylands (irrigated, fertilized) in the growing period can exceed local anthropogenic NO_2 sources, hence contributing substantially to the local tropospheric NO_x levels.

Summarizing, it may be concluded, that soil emissions of NO and HONO during the vegetation period are much more important contributors to the regional NO_2 budget (hence to regional photochemistry) of dryland regions than thought before.

Author contributions. B. Mamtimin analyzed the data and performed the estimates; B. Mamtimin and M. Badawy developed the GGTP model; B. Mamtimin and T. Behrendt carried out the field experiments; T. Behrendt performed laboratory experiments; B. Mamtimin, F. X. Meixner and T. Wagner wrote the paper. All Authors contributed to the discussion of the paper.

Acknowledgements. This work was funded through the German Research Foundation (DFG) project "DEQNO – Desert Encroachment in Central Asia – Quantification of soil biogenic Nitric Oxide" (DFG-MA 4798/1-1), the Max Planck Society (MPG). The authors like to thank Zhaopeng Wu for his field assistance and his substantial support before, during and after the field campaign. We acknowledge the free use of tropospheric NO_2 column data from the OMI sensor from www.temis.nl. We thank the Xinjiang Meteorological Bureau, PR China and United States Geological Survey for their providing meteorological data and Landsat images, respectively. The authors would like to thank S. Beirle, E. Falge, R. Shaiganfar, Y. Wang and J. Lampel for usefull discussions.

The article processing charges for this open-access publication were covered by the Max Planck Society.

ACPD
15, 34533–34604, 2015

References

Ashuri, F. A.: Der Austausch von Stickstoffmonoxid zwischen Boden und Atmosphäre unter besonderer Berücksichtigung des Bodenwassergehaltes, Einfluss kulturlandschaftlicher Verhältnisse auf den Umsatz eines Spurengases, PhD thesis, Johannes Gutenberg University Mainz, Mainz, Germany, 1–169, 2009.

Bargsten, A., Falge, E., Pritsch, K., Huwe, B., and Meixner, F. X.: Laboratory measurements of nitric oxide release from forest soil with a thick organic layer under different understory types, Biogeosciences, 7, 1425–1441, doi:10.5194/bg-7-1425-2010, 2010.

Behrendt, T., Veres, P. R., Ashuri, F., Song, G., Flanz, M., Mamtimin, B., Bruse, M., Williams, J., and Meixner, F. X.: Characterisation of NO production and consumption: new insights by an improved laboratory dynamic chamber technique, Biogeosciences, 11, 5463–5492, doi:10.5194/bg-11-5463-2014, 2014.

Beirle, S., Boersma, K. F., Platt, U., Lawrence, M. G., and Wagnet, T.: Megacity emissions and lifetimes of nitrogen oxides probed from space, Science, 333, 1739–1739, doi:10.1126/science.1207824, 2011.

Boersma, K. F., Eskes, H. J., Veefkind, J. P., Brinksma, E. J., van der A, R. J., Sneep, M., van den Oord, G. H. J., Levelt, P. F., Stammes, P., Gleason, J. F., and Bucsela, E. J.: Near-real time retrieval of tropospheric NO_2 from OMI, Atmos. Chem. Phys., 7, 2103–2118, doi:10.5194/acp-7-2103-2007, 2007.

Boersma, K. F., Eskes, H. J., Dirksen, R. J., van der A, R. J., Veefkind, J. P., Stammes, P., Huijnen, V., Kleipool, Q. L., Sneep, M., Claas, J., Leitão, J., Richter, A., Zhou, Y., and Brunner, D.: An improved tropospheric NO_2 column retrieval algorithm for the Ozone Monitoring Instrument, Atmos. Meas. Tech., 4, 1905–1928, doi:10.5194/amt-4-1905-2011, 2011.

Carlson, T., Gillies, R., and Schmugge, T.: An interpretation of methodologies for indirect measurement of soil water content, Agr. Forest Meteorol., 77, 191–205, 1995.

Chameides, W. L., Fehsenfeld, F., Rodgers, M. O., Cardelino, C.,Martinez, J., Parrish, D., Lonneman, W., Lawson, D. R., Rasmussen, R. A., Zimmerman, P., Greenberg, J., Middleton, P., and Wang, T.: Ozone precursor relationships in the ambient atmosphere, J. Geophys. Res., 92, 6037–6055, 1992.

Chander, G. and Markham, B.: Revised Landsat-5 TM radiometric Calibration procedures and postcalibration dynamic ranges. IEEE Transaction on Geoscience and Remote Sensing, Vol. 41, No. 11, 2674–2677, 2003.

ACPD
15, 34533–34604, 2015

Chander, G., Markham, B. L., and Helder, D. L.: Summary of current radiometric calibration coefficients for Landsat MSS, TM, ETM+, and EO-1 ALI sensors, Remote Sens. Environ., 113, 893–903, 2009.

Chen, S. H., Zhang, Y., Liu, J., Cui, S. S., and Shen, J. P.: Present situation, problems and countermeasure of applying fertilizer to cotton Xinjiang, Xinjiang Agricultural Sciences, 45, 147–150, 2008.

Chen, X. P., Cui, Z. L., Vitousek, P. M., Cassman, K. G., Matson, P. A., Bai, J. S., Meng. Q. F., Hou, P., Yue, S. C., Römheld, V., and Zhang, S. F.: Integrated soil-crop system management for food security, P. Natl. Acad. Sci. USA, 108, 6399–6404, 2011.

Conrad, R.: Soil Microorganisms as controllers of atmospheric trace gases (H_2, CO, CH_4, N_2O, and NO), Microbiol. Rev., 60, 609–640, 1996.

Crutzen, P. J.: Role of the tropics in atmospheric chemistry, in: The Geophysiology of Amazonia, edited by: Dickinson, R. E., John Wiley & Sons, New York, 107–132, 1987.

Davidson, E. A. and Kingerlee, W.: A global inventory of nitric oxide emissions from soils, Nutr. Cycl. Agroecosys., 48, 37–50, 1997.

Davidson, E. A., Matson, P. A., Vitousek, P. M., Riley, R., Dunkin, K., Garciamendez, G., and Maass, J. M.: Processes regulating soil emissions of NO and N_2O in a seasonally dry tropical forest, Ecology, 74, 130–139, 1993.

Delon, C., Mougin, E., Serça, D., Grippa, M., Hiernaux, P., Diawara, M., Galy-Lacaux, C., and Kergoat, L.: Modelling the effect of soil moisture and organic matter degradation on biogenic NO emissions from soils in Sahel rangeland (Mali), Biogeosciences, 12, 3253–3272, doi:10.5194/bg-12-3253-2015, 2015.

Denman, K. L., Brasseur, G. P., Chidthaisong, A., Ciais, P., Cox, P. M., Dickinson, R. E., Hauglustaine, D., Heinze, C., Holland, E. A., Jacob, D. J., Lohmann, U., Ramachandran, S., da Silva Dias, P. L., Wofsy, S. C., and Zhang, X.: Couplings between changes in the climate system and biogeochemistry, in: Climate Change 2007: The physical science basis contribution of working group 1 to the fourth assessment report of the Intergovernmental Panel on Climate Change, edited by: Solomon, S., Qin, D., Manning, M., Chen, Z., Marquis, M., Averyt, K. B., Tignor, M., and Miller, H. L., Cambridge University Press, Cambridge, 499–588, 2007.

Diallo, D. and Mariko, A.: Field capacity (FC) and permanent wilty point (PWP) of clay soils developed on Quaternary alluvium in Niger River loop (Mali), International Journal of Engineering Research and Applications, 3, 1085–1089, 2013.

ACPD
15, 34533–34604, 2015

Du, Y., Teillet, P. M., and Cihlar, J.: Radiometric normalization of multitemporal high-resolution satellite images with quality control for land cover change detection, Remote Sens. Environ., 82, 123–134, 2002.

Fechner, A.: The release of nitric oxide from agriculturally managed soils of selected oases on the fringe of the Taklimakan desert (Xinjiang, P. R. China) – Investigation of fertilizers' impact, MSc thesis, Institute of Geography, Johannes Gutenberg University, Mainz, Germany, 135 pp., 2014 (in German).

Feig, G. T., Mamtimin, B., and Meixner, F. X.: Soil biogenic emissions of nitric oxide from a semi-arid savanna in South Africa, Biogeosciences, 5, 1723–1738, doi:10.5194/bg-5-1723-2008, 2008.

Gelfand, I., Feig, G., Meixner, F. X., and Yakir, D.: Afforestation of semi-arid shrubland reduces biogenic NO emission from soil, Soil Biol. Biochem., 41, 1561–1570, 2009.

Goward, S. N. and Williams, D. L.: Landsat and earth systems science: development of terrestrial monitoring, Photogramm. Eng. Rem. S., 63, 887–900, 1997.

Goward, S., Xue, Y., and Czajkowski, K.: Evaluating land surface moisture conditions from the remotely sensed temperature/vegetation index measurements. An exploration with the simplified simple biosphere model, Remote Sens. Environ., 79, 225–242, 2002.

Hall, S. J., Huber, D., and Grimm, N. B.: Soil N_2O and NO emissions from an arid, urban ecosystem, J. Geophys. Res.-Biogeo., 113, G01016, doi:10.1029/2007JG000523, 2008.

Hao, J. M., Tian, H. Z., and Lu, Y. Q.: Emission inventories of NO_x from commercial energy consumption in China, 1995–1998, Environ. Sci. Technol., 36, 552–560, 2002.

IPCC: Climate Change 2001: The scientific basis, contribution of working group I to the third assessment report of the intergovernmental panel on climate change (IPCC), in: Chapter 4: Atmospheric Chemistry and Greenhouse Gases, edited by: Houghton, J. T., Ding, Y., Griggs, D. J., Noguer, M., van der Linden, P. J., and Xiaosa, D., Cambridge University Press, Cambridge, New York, 239–287, 2001.

Irish, R.: Landsat 7 science data users handbook, NASA Goddard Space Flight Cent., Greenbelt, Md., available at: http://landsathandbook.gsfc.nasa.gov/pdfs/Landsat7_Handbook.pdf (last access: 8 December 2015), 2003.

Jackson, T., Chen, D., Cosh, M., Li, F., Anderson, M., Walthall, C., Doriaswamy, P., and Hunt, E.: Vegetation water content mapping using Landsat data derived Normalized Difference Vegetation Index for corn and soybeans, Remote Sens. Environ., 91, 475–482, 2004.

ACPD
15, 34533–34604, 2015

Jensen, J. R.: Introductory Digital Image Processing: a Remote Sensing Perspective, 3rd Edn., Prentice-Hall, Upper Saddle River, 198–210, 337–401, 2005.
Jin, J. X. and Ma, X. D.: Xinjiang Statistical Yearbook 2009, China Statistics Press, Beijing, 2009.
Jin, J. X. and Ma, X. D.: Xinjiang Statistical Yearbook 2011, China Statistics Press, Beijing, 2011.
Kasibhatla, P. S., Levy, H., and Moxim, W. J.: Global NO_x, HNO_3, Pan, and NO_y distributions from fossil-fuel combustion emissions – a model study, J. Geophys. Res.-Atmos., 98, 7165–7180, 1993.
Kirkman, G. A., Yang, W. X., and Meixner, F. X.: Biogenic nitric oxide emissions upscaling: an approach for Zimbabwe, Global Biogeochem. Cy., 15, 1005–1020, 2001.
Kottek, M., Grieser, J., Beck, C., Rudolf, B., and Rubel, F.: World map of the Köppen-Geiger climate classification updated, Meteorol. Z., 15, 259–263, 2006.
Lai, R.: Potential of desertification control to sequester carbon and mitigate the greenhouse effect, Climatic Change, 51, 35–72, 2001.
Lambine, E. F. and Ehrlich, D.: The surface temperature-vegetation index space for land cover and land-cover change analysis, Int. J. Remote Sens., 17, 463–487, 1996.
Li, Z. X., Zhu, Z. J., Yang, L. L., Yang, Z. Q., Cui, K. B., Liu, K., Liu, J., Shen, X. H., and Maihemujiang: Study on technical countermeasure of promoting Xinjiang raisin into international market, Xinjiang Agricultural Science, 49, 129–135, 2012.
Liang, S., Fang, H., Morisette, J. T., Chen, M., Shuey, C. J., Walthall, C. L. Walthall, and Daughtry, C. S. T.: Atmospheric correction of landsat ETM+ land surface imagery: II. Validation and applications, IEEE T. Geosci. Remote, 40, 2737–2746, doi:10.1109/TGRS.2002.807579, 2002.
Lu, D., Mausel, P., Brondizio, E., and Moran, E.: Assessment of atmospheric correction methods for Landsat TM data applicable to Amazon basin LBA research, Int. J. Remote Sens., 23, 2651–2671, 2002.
Ludwig, J., Meixner, F. X., Vogel, B., and Förstner, J.: Soil-air exchange of nitric oxide: an overview of processes, environmental factors, and modeling studies, Biogeochemistry, 52, 225–257, 2001.
Mamtimin, B.: Climate of arid and semi-arid regions and the possibilities of sustainable agriculture utilization in Xinjiang (China) as an example, PhD thesis, Johannes Gutenberg University Mainz, Mainz, Germany, 1–206, 2005.

ACPD
15, 34533–34604, 2015

Mamtimin, B. and Meixner, F. X.: Air pollution and meteorological processes in the growing dryland city of Urumqi (Xinjiang, China), Sci. Total Environ., 409, 1277–1290, 2011.
Mamtimin, B., Behrendt, T., Badawy, M. M., Wagner, T., Qi, Y., Wu, Z., and Meixner, F. X.: Tropospheric vertical column densities of NO_2 over managed dryland ecosystems (Xinjiang, China): MAX-DOAS measurements vs. 3-D dispersion model simulations based on laboratory-derived NO emission from soil samples, Atmos. Chem. Phys., 15, 867–882, doi:10.5194/acp-15-867-2015, 2015.
Mao, X.Q, Xing, Y. K., Hu, T., Zeng, A., and Liu, S. Q.: An environmental-economic analysis of carbon, sulfur and nitrogen co-reduction path for China's power industry, China Environmental Science, 32, 748–756, 2012.
Markham, B. L. and Barker, J. L.: Landsat MSS and TM postcalibration dynamic ranges, exoatmospheric reflectance and at-satellite temperatures, EOSAT Landsat Tech. Notes 1, Earth Obs. Satell. Co., Lanham, Md., 3–8, 1986.
McCalley, C. K. and Sparks, J. P.: Abiotic gas formation drives nitrogen loss from a desert ecosystem, Science, 326, 837–840, 2009.
Meixner, F. X. and Yang, W. X.: Biogenic emissions of nitric oxide and nitrous oxide from arid and semi-arid land, in: Dryland Ecohydrology, edited by: D'Odorico, P. and Porporat, A., Springer, Dordrecht, 233–255, 2006.
Meixner, F. X., Fickinger, T., Marufu, L., Serca, D., Nathaus, F. J., Makina, E., Mukurumbira, L., and Andreae, M. O.: Preliminary results on nitric oxide emission from a southern African savanna ecosystem, Nutr. Cycl. Agroecosys., 48, 123–138, 1997.
Oswald, R., Behrendt, T., Ermel, M., Wu, D., Su, H., Cheng, Y., Breuninger, C., Moravek, A., Mougin, E., Delon, C., Loubet, B., Pommerening-Röser, A., Sörgel, M., Pöschl, U., Hoffmann, T., Andreae, M. O., Meixner, F. X., and Trebs, I.: HONO emissions from soil bacteria as a major source of atmospheric reactive nitrogen, Science, 341, 1233–1235, 2013.
Otter, L. B., Yang, W. X., Scholes, M. C., and Meixner, F. X.: Nitric Oxide emissions from a southern African Savanna, J. Geophys. Res., 104, 18471–18485, 1996.
Pu, Y. P.: Tulufan (Turpan) Statistical Yearbook 2009 and 2011. China Statistics Press, Beijing, 2011.
Roy, D.: Investigation of the maximum Normalized Difference Vegetation Index (NDVI) and the maximum surface temperature (Ts) AVHRR compositing procedures for the extraction of NDVI and Ts over forest, Int. J. Remote Sens., 18, 2383–2401, 1997.

ACPD
15, 34533–34604, 2015

Sandholt, I., Rasmussen, K., and Andersen, J.: A simple interpretation of the surface temperature/vegetation index space for assessment of surface moisture status, Remote Sens. Environ., 79, 213–224, doi:10.1016/S0034-4257(01)00274-7, 2002.
Schott, J. R. and Volchok, W. J.: Thematic Mapper thermal infrared calibration, Photogramm. Eng. Rem. S., 51, 1351–1357, 1985.
Shi, Y., Xia, Y. F., Lu, B. H., Liu, N., Zhang, L., Li, S. J., and Li, W.: Emission inventory and trends of NO_x for China, 2000–2020, Journal of Zhejiang University-SCIENCE A (Applied Physics & Engineering), 15, 454–464, 2014.
Skopp, J., Jawson, M. D., and Doran, J. W.: Steady-state aerobic microbial activity as a function of soil-water content, Soil Sci. Soc. Am. J., 54, 1619–1625, 1990.
Sobrino, J. A., Jiménez-Muñoz, J. C., and Paolini, L.: Land surface temperature retrieval from Landsat TM 5, Remote Sens. Environ., 90, 434–440, 2004.
Storey, C. J.: Landsat image geocorrection and registration, in: Image Registration for Remote Sensing, edited by: Le Moigne, J., Netanyahu, N. S., and Eastman, R. D., Cambridge University Press, 400–414, 2011.
Storey, J., Scaramuzza, P., Schmidt, G., and Barsi, J.: Landsat 7 scan line corrector-off gap filled product development, in: Proceeding of the 2005 American Society for Photogrammetry and Remote Sensing Pecora 16 Conference on Global Priorities in Land Remote Sensing, Sioux Falls, South Dakota, 2005.
Van de Griend, A. A. and Owe, M.: On the relationship between thermal emissivity and the normalized difference vegetation index for natural surfaces, Int. J. Remote Sens., 14, 1119–1131, doi:10.1080/01431169308904400, 1993.
Van Dijk, S. M., Gut, A., Kirkman, G. A., Meixner, F. X., and Andreae, M. O.: Biogenic NO emissions from forest and pasture soils: relating laboratory studies to field measurements, J. Geophys. Res., 107, LBA25.1–LBA25.11, 2002.
Wan, Y.: Strategy of foreign trade office of several companies to develop raisins international market. Baidu Wenku/Baidu Library published by the Government of the PR China, available at: http://wenku.baidu.com/list/146.html (last access: 14 November 2012), 2012.
Wang, X., Xie, H., Guan, H. and Zhou, X.: Different responses of MODIS-derived NDVI to Root-zone soil moisture in semi-arid and humid regions, J. Hydrol., 340, 11–24, 2007.
Weggel, O.: Xinjiang (Sinkiang), Institut fuer Asienkunde, Hamburg, Germany, 76 pp., 1985.

ACPD
15, 34533–34604, 2015

Yang, W. X. and Meixner, F. X.: Laboratory studies on the release of nitric oxide from subtropical grassland soils: the effect of soil temperature and moisture, in: Gaseous Nitrogen Emissions from Grasslands, Wallingford, England, 67–70, 1997.
Yilmaz, M., Hunt Jr., E., Goins, L., Ustin, S., Vanderbilt, V., and Jackson, T.: Vegetation water content during SMEX04 from ground data and Landsat 5 Thematic Mapper imagery, Remote Sens. Environ., 112, 350–362, 2008.
Yu, J., Meixner, F. X., Sun, W., Liang, Z., Chen, Y., Mamtimin, B., Wang, G., and Sun, Z.: The biogenic nitric oxide emission from saline sodic soils in semiarid region, Northeastern China: a laboratory study, J. Geophys. Res., 113, 1–11, 2008.
Zeng, Y., Feng, Z., and Xiang, N.: Assessment of soil moisture using Landsat ETM+ temperature/vegetation index in semiarid environment, IEEE, 6, 4306–4309, 2004.
Zhang, Q., Streets, D. G., Carmichael, G. R., He, K. B., Huo, H., Kannari, A., Klimont, Z., Park, I. S., Reddy, S., Fu, J. S., Chen, D., Duan, L., Lei, Y., Wang, L. T., and Yao, Z. L.: Asian emissions in 2006 for the NASA INTEX-B mission, Atmos. Chem. Phys., 9, 5131–5153, doi:10.5194/acp-9-5131-2009, 2009.
Zhou, X. Q.: China Electric Power Yearbook, China Power Press, Beijing, 2006.

ACPD
15, 34533–34604, 2015

Table 1. Emission factors for NO_2 for individual source* categories and fuel types (kg NO_2 t^{-1}).

Economic sector	Coal	Crude oil	Coke	Gasoline	Natural gas	Diesel
Electric power	11.8	6.35		9.4	36.47	5.32
Industry	7.5	5.3	9.0	16.7	24.0	9.62
Domestic use	1.19	1.7	2.25	16.7	14.62	14.62
Transportation			9.0	21.24	20.85	20.85
Construction	7.5		9.0	16.7	20.85	20.85

*All emission factors are in kg NO_2 t^{-1}, except natural gas, which are in 10^{-4} kg NO_2 m^{-3} (Pu, 2009; 2011).

ACPD
15, 34533–34604, 2015

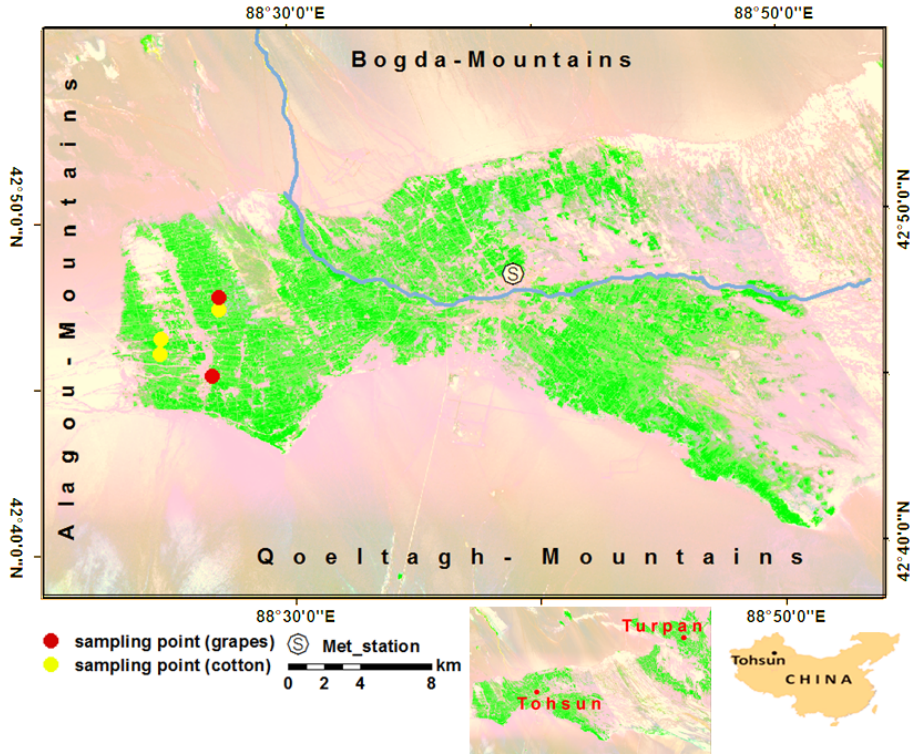

Figure 1. Satellite map of the Tohsun oasis (Landsat ETM+, 13 August 2010; "gamma correction" was appield to enhance the contrast of this Landsat image). Green color identifies arable soils of the Tohsun oasis, red and yellow dots represent the locations of soil sampling from grape fields and cotton fields, respectively. The blue line represents the seasonal Bai Yanggou River. The study area of the Tohsun oasis is approx. 50 km SW of Turpan city.

ACPD
15, 34533–34604, 2015

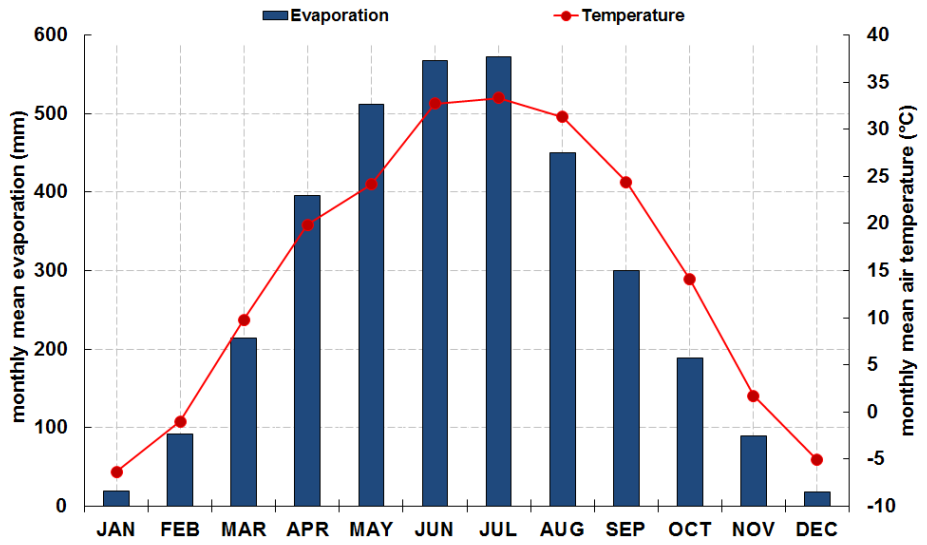

Figure 2. Climate diagram of the Tohsun oasis. Red dots represent monthly means of air temperature, blue bars monthly means of potential evaporation for the period 1971–2005 (data source: Xinjiang Meteorological Bureau, Urumqi, P.R. China).

ACPD
15, 34533–34604, 2015

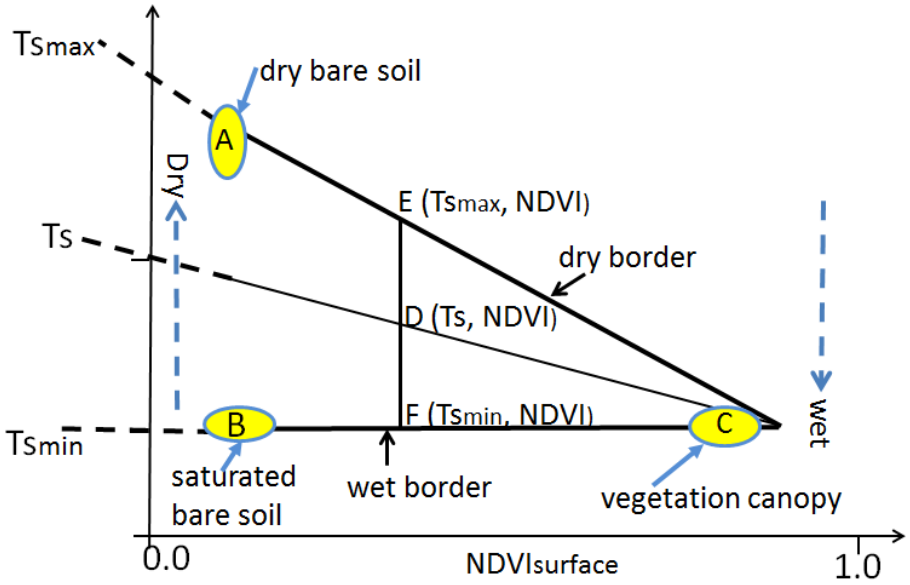

Figure 3. Simplified representation of the T_s/NDVI$_{surface}$ space (a scatter space, when plotting T_s vs. the corresponding NDIV$_{surface}$ data) used for the calculation of the soil moisture index (SMI).

ACPD
15, 34533–34604, 2015

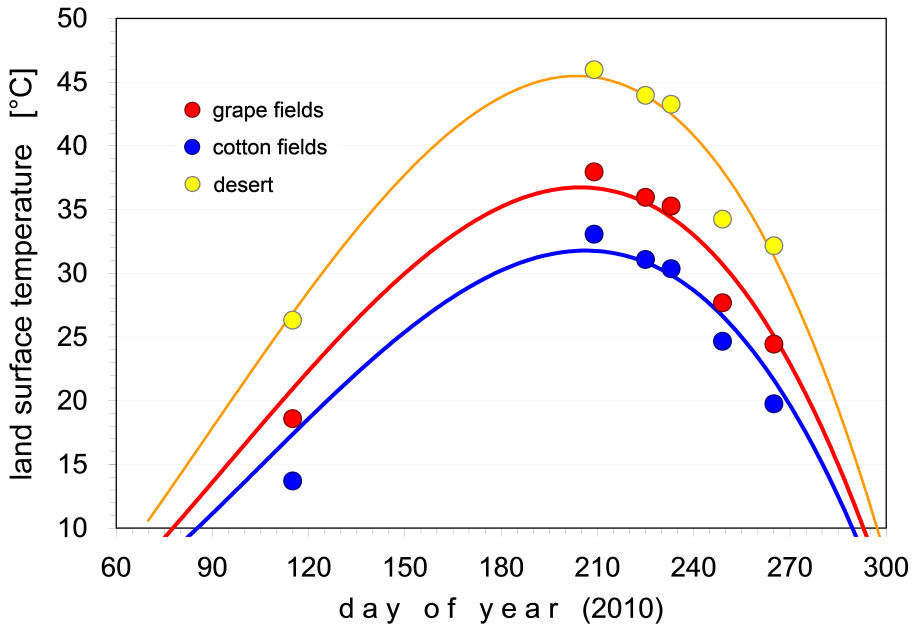

Figure 4. Land surface temperature data for the three land use types "desert", "cotton fields", "grape fields" of the Tohsun oasis as derived from Landsat images on 25 April (DOY 115), 28 July (DOY 209), 13 (DOY 225) and 21 (DOY 233) August, 6 (DOY 249) and 22 (DOY 265) September 2010 (approx. 10:45 LT). The corresponding curves represent 3rd order polynomial fits to the data (R^2 = 0.98, 0.96, and 1.00 for "grapes fields", "cotton fields", "desert", respectively).

ACPD
15, 34533–34604, 2015

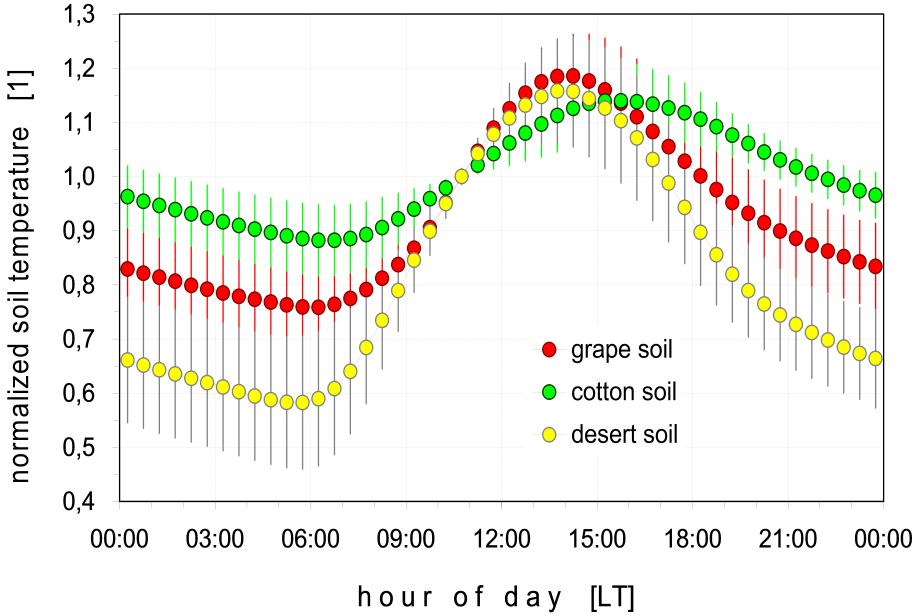

Figure 5. Mean diel variation of the normalized soil temperatures (30 min averages) for the three land use types "desert", "cotton fields", "grape fields" of the Tohsun oasis; original data (5 min) of every particular day have been normalized to the mean soil temperature observed at 10:45 LT (Landsat satellite overflight time).

ACPD
15, 34533–34604, 2015

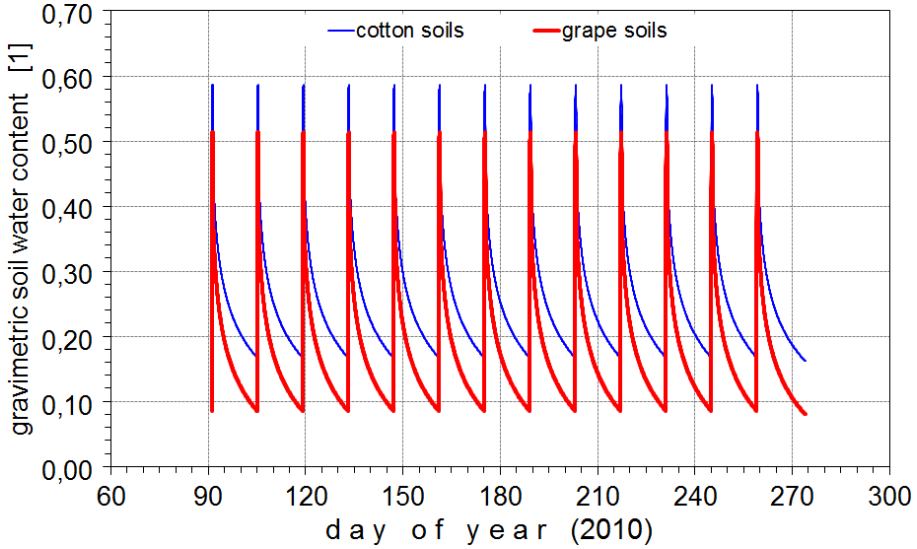

Figure 6. Seasonal variation of the gravimetric soil moisture content (at 30 min resolution) for the land use types "cotton fields" and "grape fields" of the Tohsun oasis for the entire growing period of 2010 (April–September); regular temporal patterns are due to chosen irrigation schedules (starting at 1 April (DOY 90) and repeated every 2 weeks) adapted from observations at the oases of Kuche and Minfeng (details, see text). Gravimetric soil moisture content for the land use type "desert" is assumed to be constant (0.0028).

ACPD
15, 34533–34604, 2015

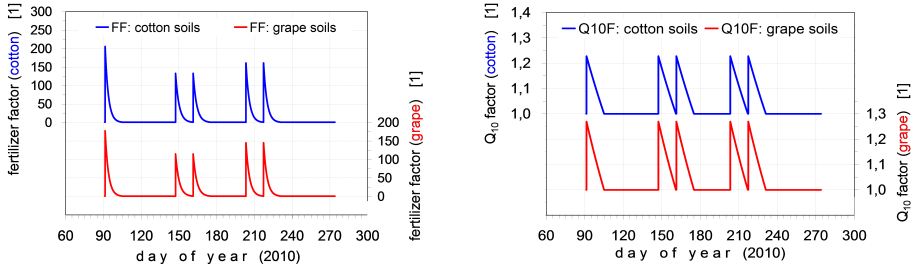

Figure 7. Seasonal variation of the (dimensionless) factors (FF and $Q_{10}F$, details s. text) which enhance the net NO fluxes of the land use types "cotton fields" and "grape fields" of the Tohsun oasis due to fertilizer application for the entire growing period of 2010 (April–September).

ACPD
15, 34533–34604, 2015

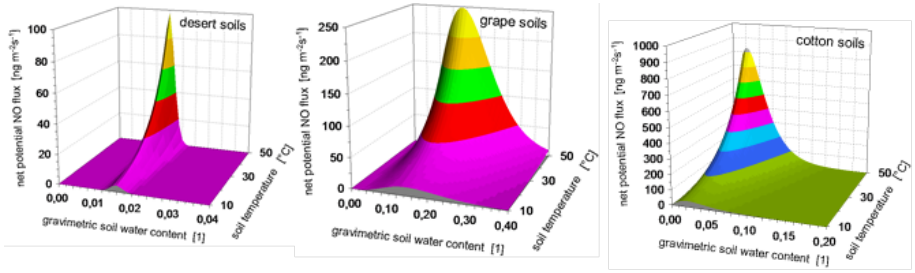

Figure 8. Results of laboratory incubation measurements on soil samples of the Tohsun oasis taken in 2010: the net potential NO fluxes F_{NO} (ng m^{-2} s^{-1}, in terms of mass of NO) from the three major land use types of the Tohsun oasis (desert, grape, and cotton soils) are shown as functions of soil temperature and the gravimetric soil moisture content. The soil samples have been taken in in 2010. Note the different scales of net potential NO fluxes and the gravimetric soil water content.

ACPD
15, 34533–34604, 2015

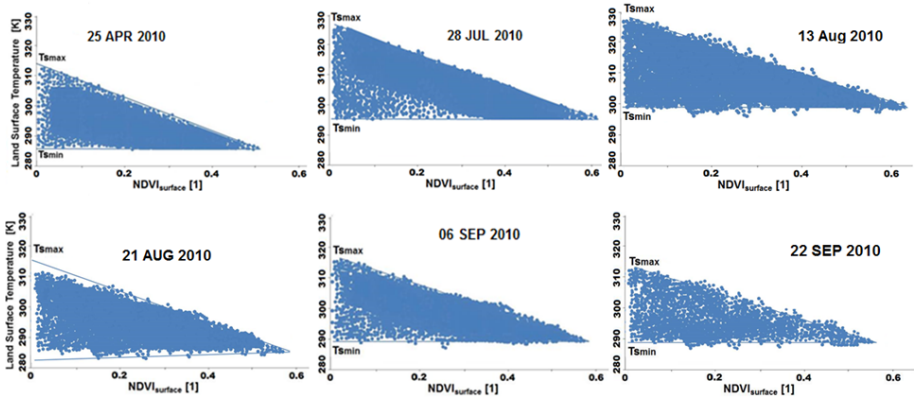

Figure 9. Scatter plots of the Land Surface Temperature T_s vs. the Normalized Differenced Vegetation Index $NDVI_{surf}$ derived from Landsat images of the Tohsun oasis on 25 April (begin of the vegetation period), 28 July, 13 and 21 August, (middle of the vegetation period), and 6 and 22 September (end of the vegetation period).

ACPD
15, 34533–34604, 2015

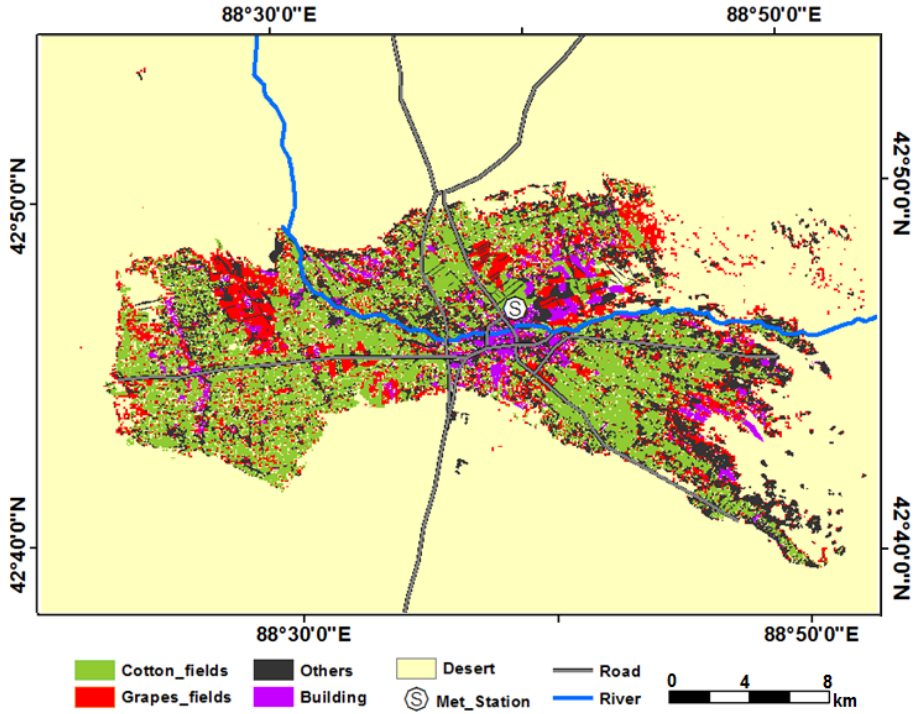

Figure 10. Land-cover classification map (2010) derived from a Landsat Image (13 August 2010).

ACPD
15, 34533–34604, 2015

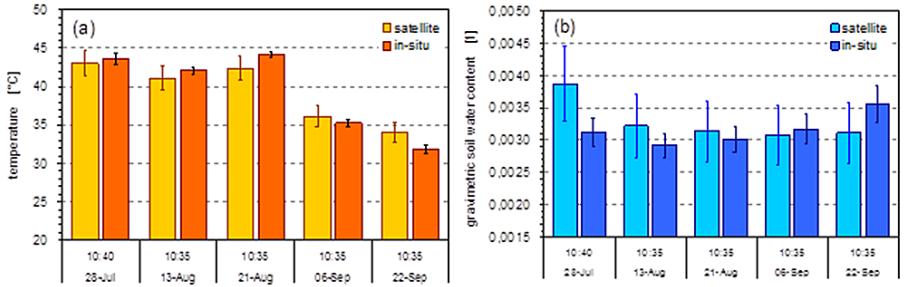

Figure 11. Satellite derived land surface temperature and gravimetric soil moisture content and results of in situ measurements (soil temperature and relative humdity of soil air at 5 cm depth) in bare soil at Tohsun County Meteorological station during July–September 2010. In-situ data of relative humdity of soil air have been converted to gravimetric soil moisture content (by laboratory calibration, s. Sect. 2.4.6). Light color bars represent the Landsat satellite data (at local time of overflight), dark color bars indicate 20 min averages of the in situ measurements (25 min time delay due to heat conductance is considered, s. Sect. 2.4.6). Error bars indicate the typical uncertainties of satellite derived data (±15 %) and the instrumental uncertainty of the in situ measurements (±5 % relative humidity of soil air), respectively.

ACPD
15, 34533–34604, 2015

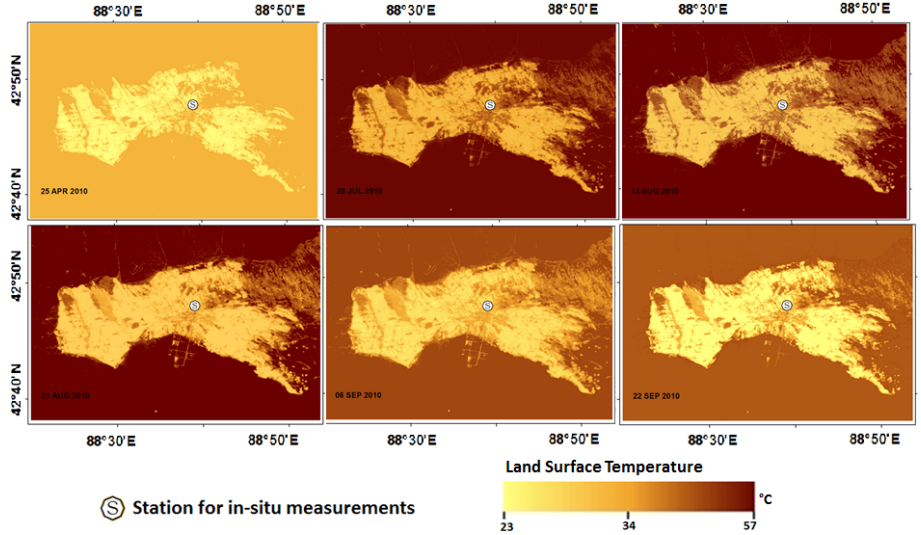

Figure 12. 2-D distributions of Land Surface Temperature (LST) of the Tohsun oasis derived from Landsat images (11:00 LT) of 25 April, 28 July, 13 and 21 August, 6 and 22 September 2010.

ACPD
15, 34533–34604, 2015

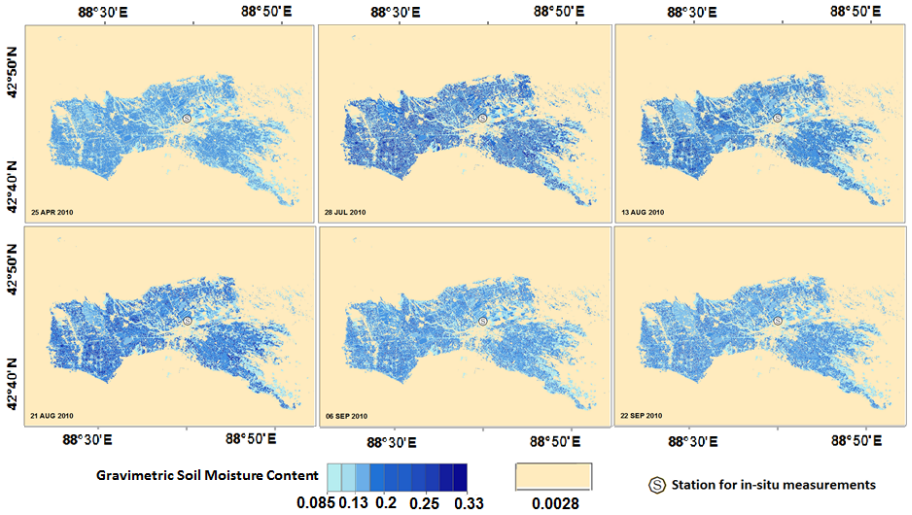

Figure 13. 2-D distributions of the gravimetric soil moisture content of the Tohsun oasis derived from Landsat images (11:00 LT) of 25 April, 28 July, 13 and 21 August, 6 and 22 September 2010.

ACPD
15, 34533–34604, 2015

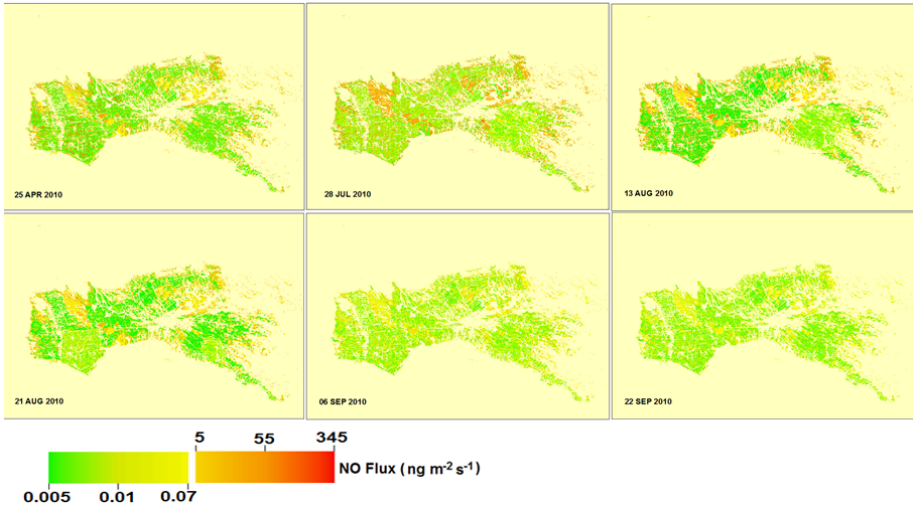

Figure 14. Results of up-scaled biogenic NO emission from the Tohsun oasis ($ng\,m^{-2}\,s^{-1}$, in terms of NO) for the beginning (25 April), the middle (28 July, 13 and 21 August), and the end (6 and 22 September) of the 2010 growing period.

ACPD
15, 34533–34604, 2015

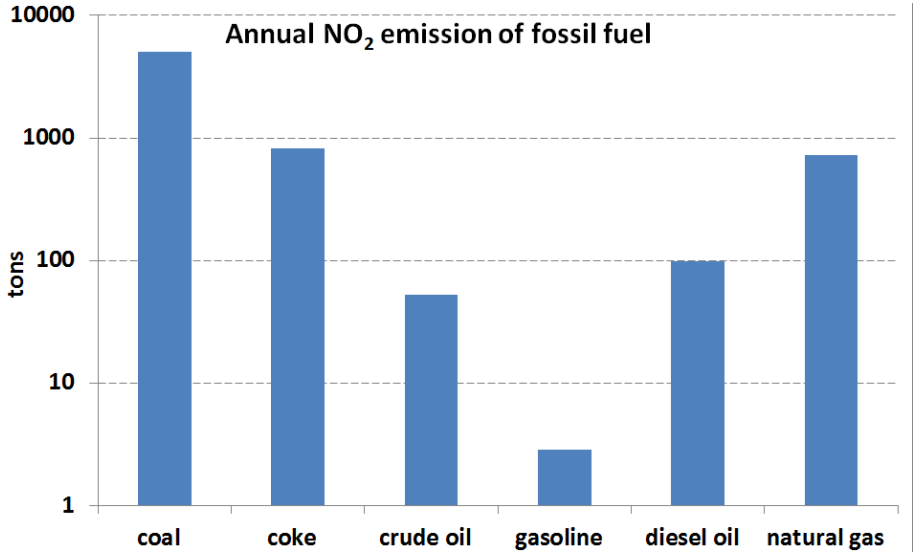

Figure 15. Annual NO_2 emission of fossil fuel of Tohsun County for 2010.

ACPD
15, 34533–34604, 2015

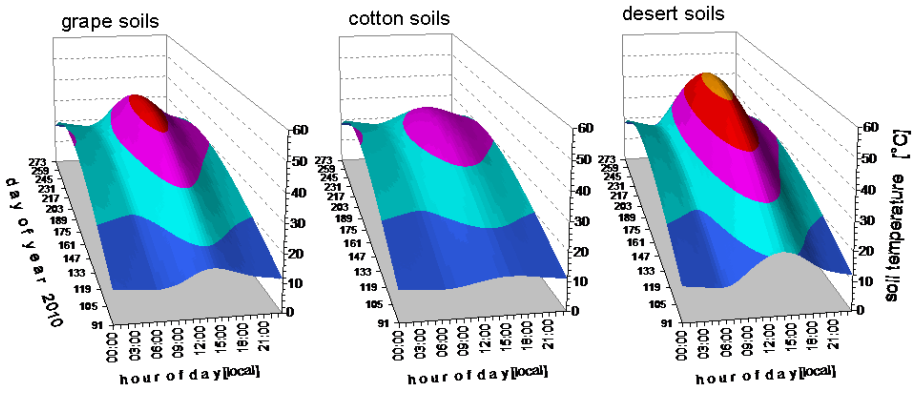

Figure 16. Seasonal variation of the diel soil temperature (30 min resolution) for "desert soils", "grape soils" and "cotton fields" of the Tohsun oasis for the entire growing period of 2010 (1 April (DOY 90)–30 September (DOY 273)).

ACPD
15, 34533–34604, 2015

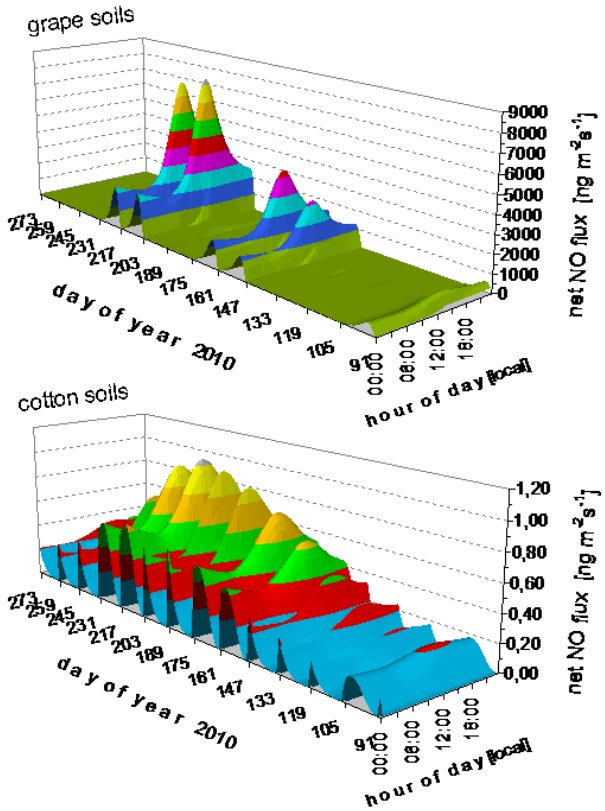

Figure 17. Seasonal variation of diel net NO flux (at 30 min resolution) for "grape soils" and "cotton fields" of the Tohsun oasis for the entire growing period of 2010 (1 April (DOY 90)–30 September (DOY 273)).

ACPD
15, 34533–34604, 2015

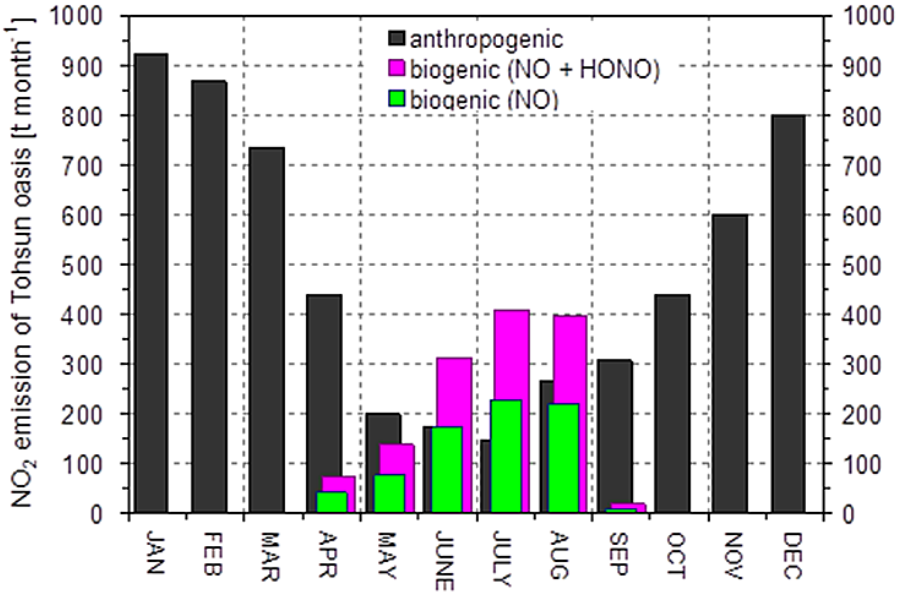

Figure 18. Anthropogenic NO_x emissions vs. soil biogenic NO_2 emissions from NO and HONO emissions of the Tohsun oasis in 2010; biogenic emissions of nitrous acid (HONO) have been estimated according to Oswald et al. (2013). All data are given in terms of mass of NO_2.

ACPD
15, 34533–34604, 2015

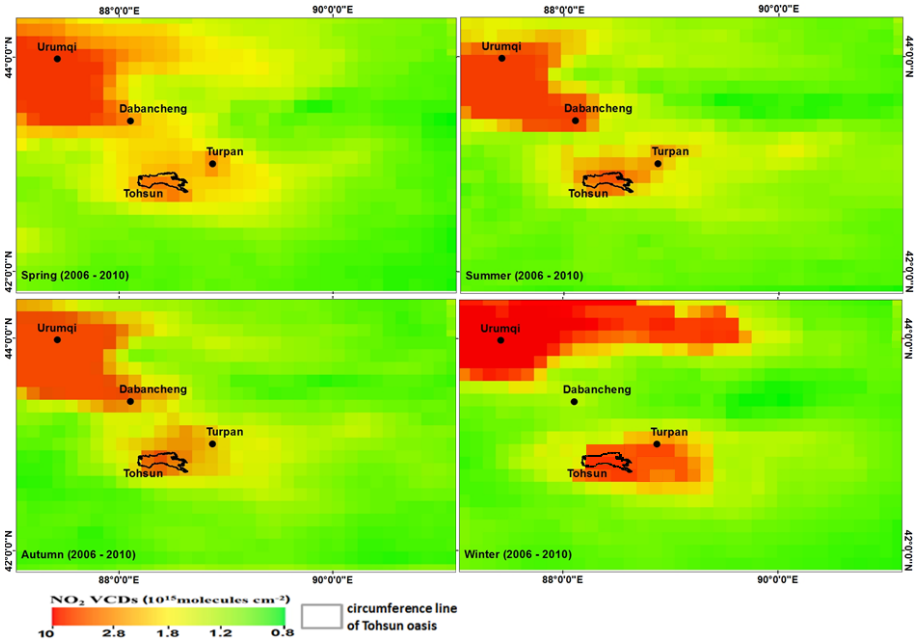

Figure 19. Seasonal 5 year-mean Tropospheric Vertical Column Densities of NO_2 (2006–2010); the "circumference line" represents the agriculturally managed part of the Tohsun oasis (230 km^2).

ACPD
15, 34533–34604, 2015

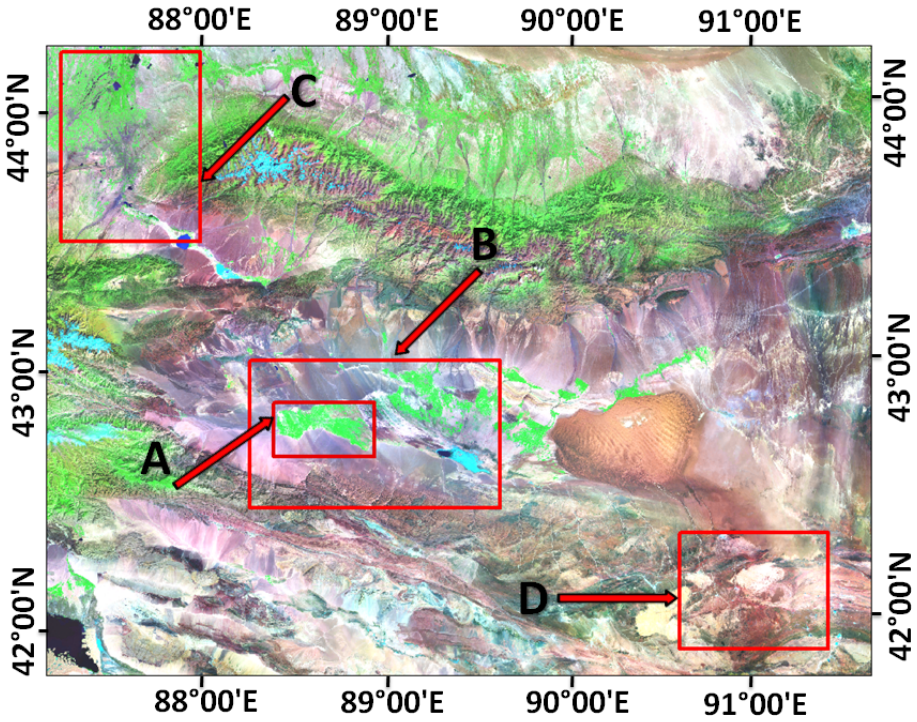

Figure 20. Selected areas for the examination of the spatial seasonal variation of the tropospheric NO_2 VCDs: rectangles "A", "B", "C", and "D" represent agricultural area (Tohsun), mixed land use area (Tohsun and Turpan city), large urban area (Urumqi) and desert area, respectively.

ACPD
15, 34533–34604, 2015

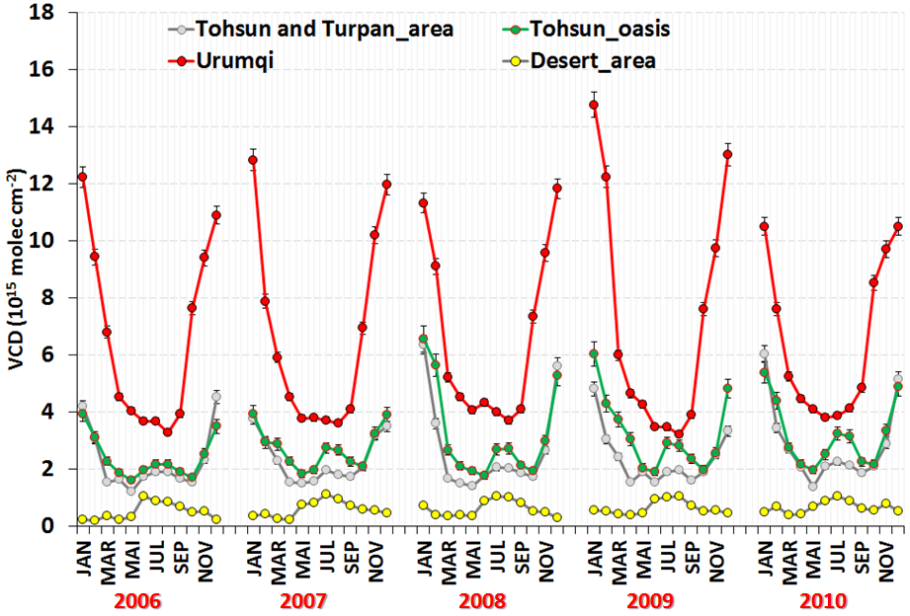

Figure 21. Monthly mean tropospheric NO_2 VCD during 2006–2010 over selected areas (unit: 10^{15} molec cm^{-2}).

ACPD
15, 34533–34604, 2015

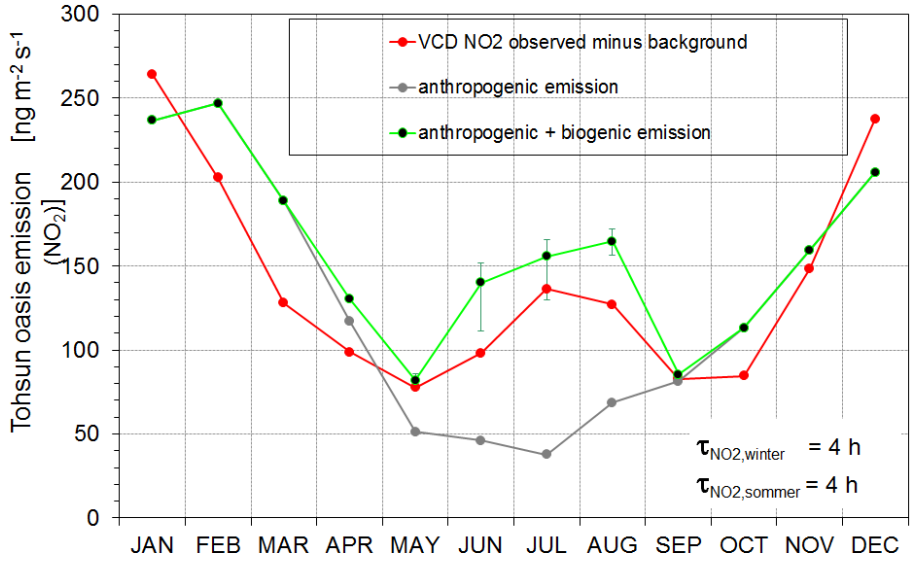

Figure 22. Monthly mean top-down emissions (from satellite observations) are compared to bottom-up (soil biogenic and antropogenic) and antropogenic emissions (in terms of ng m^{-2} s^{-1}, NO_2).

ACPD
15, 34533–34604, 2015